NASA Technical Memorandum 89027

Structural Design of an In-Line Bolted Joint for the Space Shuttle Rocket Motor Case Segments

John T. Dorsey, Peter A. Stein, and Harold G. Bush

March 1987

National Aeronautics and Space Administration

Langley Research Center
Hampton, Virginia 23665

INTRODUCTION

The Space Shuttle Solid Rocket Booster (SRB) consists of three subassemblies; the nose cone, Solid Rocket Motor (SRM) and the nozzle assembly. The SRM case consists of 11 separate weld-free steel segments (cylindrical shells) approximately 12 feet in diameter. These case segments are the forward dome section, six cylindrical sections, the aft External Tank-attach ring section, two stiffener sections, and the aft dome section. Adjoining case segments are mechanically assembled using tang-clevis joints which have 177 steel pins around the circumference of each joint (see figure 1). After machining, the six cylindrical and two stiffener sections are assembled into four separate cylindrical sections for propellant casting. Joints which are assembled in order to make the casting segments are called factory joints, and the joints between the casting segments are called field joints. An investigation by an independent Presidential Committee determined that the loss of the Space Shuttle Challenger (51-L) was most likely due to failure of the aft field joint (reference 1). A cross section view of the tang-clevis joint flown on all missions through 51-L is shown in figure 1.

The tang-clevis joints on the SRM's behave similarly to ring stiffeners on a cylindrical pressure vessel (reference 2) and achieve sealing by using the internal gas pressure to seat the O-rings. As the SRM is pressurized, the case shell wall deflects radially outwards, but the joints, because they are stiffer, deflect less. As a result, the tang and clevis portions of the joint undergo relative rotations in opposite directions, allowing a gap to open between the O-rings and the tang as shown in figure 2. The ability of the O-rings to track this gap depends on both the size of the gap and the resiliency of the O-rings. A capture tang, which is located inside the original tang (see figure 3), is added to reduce deflections between the inner arm of the clevis (with the O-rings on it) and the tang thus preventing gas flow through the joint.

This paper describes an in-line bolted concept which is an alternate way to join SRM case segments. The primary feature of the concept is that it uses a static face seal between two opposing flanges to prevent hot gas leakage. Consequently, flange pre-compression (rather than gas pressure) is used to seat the O-rings. The primary emphasis placed on the in-line bolted concept is that no gap between the two flanges in the vicinity of the O-rings is acceptable at any time prior to or during the firing of the SRM. If no gap exists, O-ring resiliency also becomes less critical since the problem of dynamically sealing a gap of varying magnitude is eliminated. Other design considerations, such as ease of manufacture, ease of assembly, and assembly verification are described in reference 3.

IN-LINE BOLTED JOINT CONCEPT

The purpose of this study is to perform a structural design and analysis of a joint concept for joining SRM case segments while meeting the following design goals and constraints. The primary design goal is to develop a joint with a static face seal, which is sealed (no gapping at the O-rings) during assembly of the segments, and remains sealed throughout the entire SRM firing.

Given this primary goal, the weight of the joint must then be minimized, and requirements concerning stress levels, ease of manufacture and assembly must be addressed. The proposed concept, show in figure 4, is similar to the bolted flange joints used in industry to connect pipes. The joint uses studs and nuts to hold opposing flanges together and to seat the two polymeric O-rings. The studs are recessed into alcoves machined into the shell wall and bearing plates are used to transfer the compressive loads from the nuts into the flanges. A shear lip helps align case segments during assembly. Gussets, which are located between the alcoves, provide a path to transfer the axial load from the shell wall to the flanges.

The structural behavior of this joint concept is directly related to values chosen for the major design variables. The particular variables studied here are; 1) the number and size of the studs used, 2) the radial location of the studs relative to the longitudinal axis of the shell wall, 3) use of a bearing plate, 4) gusset thickness, and 5) flange thickness. Assessing the joint structural behavior also requires an understanding of the applied loads. The loads that have the largest effect on joint performance in the vicinity of the O-rings for a flange design are due to the SRM firing. Following SRM ignition, the internal pressure in the SRM rapidly rises, with a maximum pressure of 988 psi occurring at the top of the rocket (reference 3). The pressure load in the SRM can be resolved into a component which acts radially outward on the shell wall, and a component that acts along the axis of the booster due to the internal pressure on the forward dome. As previously described, the radial pressure loading causes the joint to open up on the inside where the O-rings are located (see figure 2). A successful joint design will eliminate this tendency to gap in the vicinity of the O-rings.

The number of studs necessary to carry the axial load due to pressure can be estimated by multiplying the pretension load in each stud by the number of studs, and then dividing by the total applied load. The resulting clamping ratio is defined as the total axial force due to stud pretension divided by the total axial force due to internal pressure. The maximum permissible pretension load that can be carried by each stud is defined as 70 percent of the stud's ultimate load. The mimimum number of studs versus clamping ratio is calculated for four different stud sizes and shown in figure 5. The material properties of the studs, as well as the other materials considered for this design, are shown in table 1. (All parts used in this design are either previously qualified for use on the Shuttle system, or are made from qualified materials.) For a 1" diameter stud and clamping ratio=1.4, the number required is seen to be approximately 180 studs. The maximum number of studs chosen is limited by the stress in the gussets since as the number of studs is increased, the thickness of the gusset is decreased.

The size of the studs chosen has a large effect on the design of the joint concept. Larger studs weigh more and require a wider flange than smaller studs in order to provide sufficient bearing area for the nuts (see Table II). Widening the flange adds weight and increases the hoop stiffness at the joint, resulting in larger gap openings at the O-rings as shown in the bottom right of figure 6. Because of the effect of increasing stud size on the weight and hoop stiffness, it is desirable to use the smallest studs possible. If too small a stud size is chosen however, the minimum number of studs required to carry the

load increases to the point where the gusset thickness falls below acceptable levels for load transfer. The minimum number of studs required is not necessarily a good design because if the studs are spaced too far apart, a scalloping effect will result in gaps opening under the gussets due to the axial load. The scalloping effect is shown by the dashed lines underneath the gussets in the bottom left of figure 6. In order to minimize scalloping, studs are added to the minimum required up to a maximum number, with the maximum number determined by the amount of total gusset area required to keep gusset stresses to an acceptable level as shown in the top of figure 6.

Figure 7 illustrates effects of having the stud centerline offset relative to the center of the shell wall. This offset is referred to as eccentricity with a positive value occurring when the stud centerline is radially outside of the shell wall centerline. The dashed lines represent the shape of the deflection of the joint section under the individual loadings. The pressure load component will always act to open the inside of the joint where the O-rings are located, no matter what value of eccentricity is chosen. Negative eccentricity however, can be used to to transfer the axial load component from the shell wall into the gusset and create a moment about the stud to close the joint in the vicinity of the O-rings. The amount of negative eccentricity required to close the joint will depend on values chosen for the other design parameters. Eccentricity has the largest effect on joint performance for a given stud size and is therefore the first design variable to be studied after choosing a stud size.

In addition to considering eccentricity and stud size, the constraints due to the size of the metal ingots used to make the case segments must also be addressed. This constraint limits the maximum size of the studs due to the flange width. The shear lip must fit within the envelope of the metal ingot while still providing sufficient gusset material for the load transfer. The eccentricity must also be considered for its effect on gusset thickness as well as the envelope of the metal ingot. Negative eccentricity moves the stud centerline inward and results in a reduced shell circumference at the stud centerline. The smaller circumference leaves less gusset material for a given number of studs and nuts.

Gusset thickness is also a function of whether or not a bearing plate is used. Figure 8 shows the relationship between gusset thickness and nut size for both the solid flange and bearing plate concepts. The bearing plate has two purposes. First, a bearing plate allows a thicker gusset for a given stud and nut size because the fillets required at the bottom of the alcove are moved away from the nut. The distance from the stud centerline to the gusset wall in the solid flange design, d_1 in figure 8a, is larger than the same measurement, d_2 in figure 8b, for the bearing plate design. The bearing plate design allows the use of a smaller clearance between the nut and the gusset (see insets), resulting in a thicker gusset and reduced stresses. Second, for a given total thickness, a bearing plate plus flange combination will have less hoop stiffness than a solid flange. Reduced hoop stiffness is beneficial because it helps close the joint in the region of the O-rings. The thicker gussets allowed by the bearing plate do however result in more material in the gusset and thus, tends to increase the hoop stiffness at the gusset and increase joint weight. Reducing hoop stiffness in the flange region with the bearing plate is

of sufficient benefit in terms of joint closure and reduction of gusset stresses to overcome the disadvantage due to increased hoop stiffness in the gussets.

In order to ease assembly and verify the integrity of the joint, the seals should be visible from the exterior of the SRM during assembly. This is accomplished by placing the shear lip (used for alignment) on the inside of the joint and the seals in the flange between the stud and the shear lip. The seals can then be observed throughout the assembly process up to the point where the flange surfaces make contact.

Studs are used instead of bolts in the design to reduce weight. The lower weight of the stud design is due to the smaller alcove height required. As seen in figure 9, the constant diameter stud requires less room in the alcove for installation than a bolt because of the increased diameter of the bolt head. The procedure for tightening either the stud or the bolt is the same.

FINITE ELEMENT MODELING AND ANALYSIS

In this section of the paper, the various finite element model components, their assembly into a complete model, boundary conditions, and applied loadings are described. The purpose of the finite element analysis is to assess the performance of the in-line bolted joint concept as some of the major design variables are altered. This leads to the combination of design parameters which gives the best performance for the minimum weight. The software tools which are used for model construction and analysis are also discussed.

Model Description

The joint geometry is assumed to be identical at each stud location around the circumference of the booster, and the applied loadings are all symmetric. These two assumptions imply that the joint behavior will be symmetric about a plane passing through central axis of the booster and the stud centerline, and symmetric about a plane passing through the central axis of the booster and center of the gusset. Thus, only a sector of the total booster (from the centerline of a stud to the center of an adjacent gusset) needs to be modeled. In addition, a plane of symmetry is assumed at the interface between two case segements so that only the top (or bottom) half of a joint has to be analyzed. Finally, the displacements and stresses become uniform in the shell wall away from the joint. A cylindrical pressure vessel with a ring stiffener, where the pressure vessel is given stiffness properties of the SRM case and the ring stiffener given the stiffness of a tang-clevis joint is analyzed. The results (given in figure 10) show that the shell displacement becomes uniform at a height of approximately 22 inches. Thus, the joint model only has to include the first 22 inches in length from the case segment interface.

In order to simulate the contact problem between two joint halves and also to predict the general three dimensional stress state throughout the joint and shell, solid three dimensional elastic finite elements are selected for the analysis. The structural analysis code Engineering Analysis Language (EAL) is

used for all analyses and has 3 dimensional elements which are based on the assumed-stress hybrid formulation (reference 4). The contact problem between two joint faces is modeled using a nonlinear spring element (reference 2). The processor which does the gap analysis is specifically developed for, and incorporated into, EAL and is described in more detail in reference 2.

In order to characterize the joint behavior for various design parameters, a parametric study must be done. This requires that a large number of different models be rapidly created and analyzed. The modeling process is made easier by using the software package GEOMOD (reference 5) to build a 3-dimensional solid model of the joint and then using the GEOMOD mathematical description as input to SUPERTAB (reference 6) where the finite element discretization is performed. Output from SUPERTAB is translated into EAL node location and mesh connectivity input. Perturbations in design variables can then be made rapidly by changing only the joint locations part of the input and keeping all of the mesh connectivities, boundary conditions, loading inputs, gap definitions, etc. the same.

The finite element model consists of two or three separate components; the flange/gusset/shell, the stud/nut, and the bearing plate, as shown in figure 11. In the initial studies, a coarse mesh is used to study a large number of effects without incurring a large computational expense. Also, no bearing plate is used, so that the total model consists of the flange/gusset/shell plus the stud/nut. The bearing plate is used to obtain more gusset width for a given nut size and its effects are studied in a second generation model which includes all three components. Including the bearing plate increases both the total number of elements as well as the total number of nonlinear springs in the analysis. As a result, computer run times are longer for the refined model than for the coarse model.

Model assembly - Complete structural models of the joint are made by assembling the required components using nonlinear gap elements and zero length rigid elements. Physically, the bearing plate acts as a form fitted washer which is not mechanically attached to the top of the flange. Thus, nonlinear gap elements are used to connect nodes on the bottom of the bearing plate to coincident nodes on the top of the flange as shown in figure 12a. Because the gap element is essentially rigid in compression ($k = 10^8$ lb/in), but has no stiffness in tension ($k = 10^2$ lb/in), the bearing plate can transmit compressive forces from the nut to the flange, but if the bearing plate wants to pull up from the flange, no forces are applied, which is the proper physical behavior.

The stud/nut component must be attached to either the top of the flange, or if a bearing plate is present, to the top of the bearing plate. In either case, it is assumed (and later proven correct) that the top of the nut remains in contact with the top of the flange or bearing plate under all loading conditions. Thus, the added complexity of gap elements are not required in this region and rigid zero-length axial stiffness elements are used. However, unlimited relative radial motion can still take place between the stud and the flange whereas physically, relative motion should be limited to whatever tolerance exists between the two components (assumed to be .005"), after which contact occurs. This feature is incorporated into the model by defining a gap

element that allows .005" of relative closure between adjacent nodes on the stud and flange before becoming rigid. These elements are used to connect the radial degree of freedom of nodes on the $\theta=0^{o}$ plane as shown in figure 12b. Contact between the stud and flange should not occur unless there is severe bending in the flange, something which does not take place for any of the design variations studied. If contact between the stud and flange is anticipated however, gap elements should be put around the entire circumference of the stud to achieve accurate simulation of the stud bearing surface.

Boundary conditions - Assuming circumferential symmetry reduces the joint model to a sector of the motor case. The proper boundary conditions require constraining the circumferential degree of freedom at each node on the two theta planes (see figure 13). All of the nodes on these two planes are free to move in the radial and Z directions however. Because the joint model is a wedge, any movement in the radial direction will result in the application of circumferential boundary forces on the two theta planes, and thus, no constraints are required in the radial direction. Assuming symmetry at the interface of two SRM segments requires that all nodes at the bottom of the stud be constrained in the Z direction. These nodes are allowed to move in the radial and circumferential (unless on the theta = 0 plane) directions however. No constraints in the Z direction are required for the flange bottom because the gap elements assure that these nodes do not penetrate the Z symmetry plane.

Applied loadings - Two case segments are assembled by bringing the two opposing ends together such that the flange bottoms are in contact, aligning the cases so that the studs can be inserted into the holes, and attaching nuts to both ends of the stud. The nuts are then tightened until the stud is prestressed to 70 percent of its ultimate strength, with the induced force clamping the two booster segments together. This loading condition is simulated in the finite element model by using a thermal prestress. The elements which make up the stud are given a coefficient of thermal expansion in the Z direction only. A negative temperature is applied to the model which causes the stud to contract in the -Z direction. Because the nut and stud are modeled as one component, the nut must also move in the -Z direction and applies forces to the top of the flange or bearing plate. This puts the flange into compression and preloads the joint. At the same time, the stud is put into tension which results in reactions at the bottom of the stud in the Z direction. The temperature is adjusted such that the sum of the reactions at the bottom of the stud equals 0.7 times the stud's ultimate load.

After the stud preload is applied to the joint, loads corresponding to the internal pressure of 1000 psi are applied. A pressure load of 1000 psi, which always acts normal to internal booster surfaces, is applied to the inside wall of the booster in the radial direction as shown in figure 13. The internal pressure, by acting on the forward dome of the SRM, also induces an axial load in the shell. The total axial load due to 1000 psi of internal pressure is approximately 16.5 million lbf, or 36,300 lbf per inch circumference of the booster. The axial load is distributed along the top of the shell wall as an equivalent pressure load acting in the +Z direction as shown in figure 13. These particular loading conditions are chosen so as to be consistent with those reported in reference 2.

As stated previously, both of the O-rings are made of a polymeric material. The O-rings are compressed when opposing joint halves are mated during asembly, resulting in a force of approximately 25 lb/in/seal acting to open the joint (see reference 3). Since the magnitude of the O-ring force is so small relative to all other applied forces, it is not included in the analysis.

Joint Structural Performance

The primary objective, as stated in the introduction, is to design a joint which stays closed during the entire firing of the SRM. In particular, it is the area between the O-rings and the inside of the booster which must maintain zero gap under the applied loadings. Consequently, in the initial parametric studies, emphasis is placed on determining the range of design variables which close the inside of the joint. At this point, secondary emphasis is placed on stress analysis with the thought being, if the joint is not closed, the stresses are unimportant. Any locations where high stresses occur are addressed in refined models after values for the major design variables are chosen. Thus, displacement and gap results will be discussed first followed by a discussion of the joint stresses and joint weight.

Displacements and gaps - Key locations on the flange bottom of the coarse model are shown in figure 14. Locations 1050, 1070 and 1080 are on the inside edge of the SRM, locations 1071 and 1081 are on a line approximately half way between the two O-rings, and location 1085 is on the outside edge of the booster under the center of the gusset. The line formed by locations 1080, 1081, and 1085 is halfway between adjacent stud centerlines.

Based on the discussion of figure 7, it is anticipated that the stud eccentricity (the offset between the stud centerline and the shell wall centerline) will have the most dramatic effect on the joint gap performance and thus, is examined first. In the analysis, the displacements given by the nonlinear springs on the flange bottom are only the distance between the flange and the symmetry plane. Thus, the total gap between two opposing joints is actually twice the nonlinear spring displacent and it is this proper gap value which is given throughout this report. The coarse model is used for this study and has the following joint properties; 170-1 1/16" studs, 1" thick flange, and stud preload = 0.7 F_{ULT}.

In figure 15, gaps at various locations on the flange bottom are shown as a function of stud eccentricity (negative values indicating that the stud centerline moves inside the shell wall towards the shell axis) for the case of an unmodified and a split flange. The gaps on the inside of the joint decrease dramatically as the stud centerline moves inward towards the shell axis, with the location under the gusset center (1080) decreasing from 9.07 mils for eccentricity = 0", to 0.34 mils at eccentricity = -.5". At the approximate O-ring location (1081) the gap is only 0.12 mils for eccentricity = -.5". The gap at location 1050, which is also on the inside wall of the booster, closes at an eccentricity of -.4". As is expected, a point on the bottom of the flange located on the outside of the joint (1085) shows an increasing gap with increasing negative eccentricity. In figure 16 the contact region of the

flange bottom is shown for eccentricity = 0" and eccentricity = -.5". As eccentricity moves in the negative direction the contact region between two opposing flanges moves from the outside of the joint to the inside of the joint. Although an inside corner is shown not to be in contact in figure 16b, all of the gap values at this corner are less than .35 mils.

One effect of the flange is to increase the hoop stiffness locally at the ends of each SRM segment. As a result, the flange does not undergo as much radial displacement as the shell wall does away from the joint, which tends to peel up the inside of the joint and cause larger gaps in the area of the O-rings. An easy way to reduce the flange hoop stiffness is to cut or split the flange along the plane of the stud centerline outboard of the stud as shown in figure 14. In the finite element model, this effect is simulated by simply removing the constraints in the theta direction on the nodes in this area as indicated in the figure. Figure 17, which shows the radial displacement of nodes on the inside wall of the model from the flange bottom to the top of the shell, illustrates that splitting the flange allows the flange radial displacement to more closely approximate the shell displacement.

Figure 15 shows that the desired effect of decreasing gaps on the inside of the joint for a given eccentricity value by splitting the flange is also accomplished. Now the gap at location 1080 falls below 0.5 mil at an eccentricity value of -.2" compared to a value of -0.5" before. Splitting the flange reduces the bending stiffness as well as the hoop stiffness however, which results in larger gaps on the outside of the joint, 4.56 mils versus 6.56 mils for location 1085 at an eccentricity of -0.5" for example. Since the gaps on the outside of the joint are not critical however, this should be of no concern. Two reasons for minimizing the value of eccentricity are; 1) the joint weight is reduced and, 2) the amount of internal volume and thus solid fuel displaced is reduced.

The sensitivity of gap values to the amount of preload in the stud is summarized in figure 18. The gaps on the inside of the joint (at locations 1070 and 1080 on figure 18a) decrease their already small values as the stud preload is decreased from 0.7 to 0.6 F_{ULT}. Since preloading the stud pulls the inside corner of the flange under the gusset up (see figure 16), reducing the preload results in reduced gaps at this corner. These results indicate that the amount of stud preload dominates the gap behavior in this region rather than the internal pressure loading. The reduced stud preload results in slightly larger gaps on the outside of the joint however, as shown in figure 18b for location 1085.

In Table IV, gaps at the inside of the joint are shown for the cases of 180-1", 170-1 1/16", and 166-1 1/16" studs. The model used here has a solid 1" thick flange (no bearing plate), eccentricity = -.5", and a stud preload of 0.7 F_{ULT}. The results show that increasing the number of studs results in decreasing gaps at the inside of the joint for the range of studs shown. It should be remembered however, that increasing the number of studs decreases the gusset width which results in increased gusset stresses and eventually, when the gussets become thin enough, increased gaps at the inside of the joint (see discussion of figure 9). In this design study, 1" studs are found to be the smallest practical when the tradeoff between total stud area and total gusset

area is considered. The design with 170 - 1 1/16" studs is still analyzed however, to provide a point of comparison.

Including a bearing plate in the model has the desireable effect of increasing the gusset width for a given stud spacing (as discussed in figure 9) and its effects on joint gap performance are investigated next. For a given total thickness, a combination flange plus bearing plate will have less bending and hoop stiffness than a solid flange, with the stiffness reductions dependent on the ratio of bearing plate to total thickness. In Table III, gap performance for a joint with a solid 1" thick flange is compared to joints with 3/4", 1" and 1 1/4" thick flanges all with a 1/4" thick bearing plate. All four joint configurations have 170-1 1/16" studs, eccentricity of -.5" and a stud preload which is 70 percent of ultimate.

Results for the case of a solid flange and flange plus bearing plate with equivalent thicknesses (1 inch), are as anticipated. For the flange plus bearing plate model, gaps on the inside of the joint (locations 1070, 1071, 1080, and 1081) are smaller than corresponding gaps on the solid flange model due to the reduced hoop stiffness of the joint, while the gap on the outside of the joint is larger (location 1085) because of reduced bending stiffness. For a solid 1" thick flange and a 1" flange with a 1/4" bearing plate, the flange plus bearing plate model has gaps on the inside of the joint which are approximately 30 percent larger than corresponding gaps on the solid flange model. The reason for this behavior is related to the flange bearing plate combination having a gusset which is .633" wide compared to only a .483" wide gusset for the solid flange case. The increased gusset width for the flange plus bearing plate case results in greater hoop stiffness which causes larger gaps to occur on the inside of the joint as discussed in figure 9. Further increases in flange thickness (up to 1 1/4") result in larger gaps on the inside of the joint (locations 1070 and 1080), but as the flange bending stiffness increases, smaller gaps on the outside of the joint (location 1085).

At this point, the joint behavior due to changes in eccentricity, stud size, and number of studs is well understood. Since the number of design parameters being varied along with the number of computer runs can thus be reduced, the fidelity of the finite element mesh can be increased and more joint features incorporated into the model. In particular, the finite element model now includes the two O-ring grooves and the shear lip on the inside of the joint as shown in figure 19a. This same model is used to represent the opposing joint half (which just has a flat surface on the bottom) by adding elements in the O-ring grooves which have the same stiffness as the flange and removing elements representing the shear lip (see figure 19b).

Because the O-ring grooves are now included in the model, an important modification must be made in the pressure loading distribution. The assumption is made that even if the gap is zero at the inside of the joint, pressure can pass to the inside O-ring (and no farther as long as the O-ring maintains a seal). Thus, the pressure loading is now distributed along the bottom and inside surfaces of the shear lip and along the bottom of the flange to the inner O-ring groove as shown in figure 19a. On the flat side of the joint, pressure loading is included on the bottom of the joint to the point where the opposing O-ring makes contact (see figure 19b).

Although gaps were monitored at all locations on the flange bottom of the refined model, the locations shown in figure 20 are more important and will be discussed subsequently. Locations 301 and 383 are on the inside edge of the booster, locations 302 and 384 on the inside edge of the inner O-ring groove, 305 and 387 on the inside edge of the outer O-ring groove, and 312 and 396 on the outside edge of the joint. Gap locations are identical for the O-ring and flat sides of the joints.

In Table V, gaps on the flange bottom are compared for a joint with a 1" thick flange (flat side) and an 3/4" thick flange (O-ring side). The specific design parameters in this model are; 170-1 1/16" studs, eccentricity = -.5", bearing plate thickness = .25", and stud preload = $0.7F_{ULT}$. Very small to zero gaps on the inside edges of the O-ring grooves for both designs indicates no advantage in going to the heavier 1" thick flange design. The larger 9.2 mil gap at the outside edge of the joint with the 3/4" thick flange is noted, but is not significant in terms of joint performance.

Gap performance on the O-ring side of the joint is compared for the 170-1 1/16" and 180-1" stud designs in Table VI. Both joints have 3/4" thick flanges, 1/4" thick bearing plates, eccentricity=-.5", and stud preload = $0.7F_{ULT}$. The gap performance is essentially the same for both joints, with no gaps occurring on the inside edges of the O-ring grooves and 8 to 9 mil gaps occurring under the gusset at the outside of the joint.

In Table VII, gap performance is shown for various cases of a joint design which has 180-1" studs, 3/4" thick flange, 1/4" thick bearing plate, and stud preload = $0.7\ F_{ULT}$. (All entries referring to slots will be discussed in the section on stresses.) The first two entries establish the baseline performance of the 180-1" stud design and show that the behavior of opposing joint halves is identical (that is, the O-ring grooves and shear lip did not cause any changes in joint behavior). This serves to validate the study results obtained with the coarse finite element models which did not include the O-ring grooves. The results show that the primary objective stated in the introduction, to design a joint which does not allow any gaps to occur at the O-rings during firing of the rocket booster, has been met.

Stresses - Stresses in the model are also monitored during the joint parametric studies but not assessed until a combination of design parameters are determined which keep the inside of the joint closed. In general, the model has sufficient fidelity to accurately predict stresses where stress gradients are small but where stress gradients are large, the model will predict stresses less accurately. For example, when two pieces intersect at right angles in the physical structure, filets are put in to alleviate any stress concentration at the corner. The models described in this paper however, have fairly coarse finite element meshes and no filets are modeled. Thus, the likelihood of stress concentrations occurring at sharp corners exists. The stress data therefore, must be interpreted with such modeling limitations in mind. All stresses quoted in this report are element bulk stresses, which are calculated by averaging the element nodal stresses (8 corners of a brick, 6 corners of a wedge, and 4 corners of a pyramid).

Acceptable stress levels in the model were defined by dividing the material tensile ultimate by a factor of 1.4. Material stresses in the shell wall, gusset, and flange must therefore be equal to or less than 139 ksi, stresses in the bearing plate and nut must be equal to or less than 189 ksi, stresses in the stud must be less than 195 ksi. Locations in the shell, gusset, or flange where stresses exceed 139 ksi are shown in figure 21 and specific stress values for a design with 170-1 1/16" studs, eccentricity=-.5", and bearing plate thickness = 1/4" are shown for three flange thicknesses in Table VIII.

The first area of high local stress occurs where the wedge, which makes the transition from the shell wall to the gusset, intersects the gusset (location A in figure 21). The gusset runs straight into the wedge with no tapering and thus a sharp corner exists. The highest stress value in this location is 149 ksi. A slight taper was easily added to the model and the maximum stress in this region dropped to an acceptable value of 134 ksi.

A second area of high stress exists at the top of the alcove where the top of the wedge intersects the shell wall (location B in figure 21). Once again, no tapering or fileting is done in this region so that a sharp corner exists which results in the stress being 185 ksi in the particular element shown. Due to the complicated nature of the model in this region however, the elements could not be easily modified to show how sculpturing and tailoring material would reduce the stress level to an acceptable level. The results obtained at location A indicate that the stress at location B could be successfully reduced by refining the geometry and finite element mesh of that particular region in a new model.

The stress concentration at location C is of an entirely different nature however, because it results from the physics of the joint loading. Recalling the classical problem of an infinite plate with a hole in the center and loaded in uniaxial tension, the results indicate that a stress concentration occurs at the edge of the hole and has a value which is three times the far field stress. This problem is reproduced in the SRM joint, with the flange (having a very large radius of curvature) acting like a finite width plate and the circumferential stress induced by the internal booster pressure simulating the uniaxial tension load. The joint loading is actually more complicated because bending in the flange due to the axial loading also takes place, but the stress concentration around the hole is reproduced as shown by the values for location C1 and C2 in Table VIII. The largest stress, 278 ksi, occurs on the outside bottom edge of the hole for the 3/4" thick flange design. The stress concentration decreases slightly to 227 ksi as the flange thickness is increased to 1 1/4". At this point in the in-line bolted design however, the importance of the stress concentrations at location C cannot be judged due to lack of information. In particular, analyses which include plasticity effects and a number of load cycles need to be run on the joint to completely characterize its performance.

If the stress concentration around the hole proves unacceptable, a method for reducing those stresses does exist. The observation is made that if slots are cut in the flange tangent to the hole in the circumferential direction and extended to the gusset, the flange will look like two concentric rings, thus

removing the stress concentration. This idea was incorporated into the finite element mesh for the refined model and is shown pictorially in figure 22. The bearing plate takes on increased importance in this model because it now must transfer the nut bearing load to the inner and outer rings and the middle tab while having enough stiffness not to deform significantly where it spans the slots. The tab of material between the inner and outer rings is purposely left so that the bearing plate does not have to span too large a distance and also to aid in holding the middle of the gusset down. In this model, the bearing plate also helps to center the stud in the flange.

The effect of cutting slots in the flange are shown in Table IX for a design which has 180 - 1" studs, eccentricity = -.5", flange thickness = 3/4", and bearing plate thickness = 1/4". The slots result in a 23 percent reduction in maximum flange stress, from 340 ksi to 262 ksi. Also, the slots are seen from Table VII to cause a negligible increase in gaps on the inside of the joint and only a 3 mil increase in gap on the outside of the joint. Cutting slots and then splitting the flange causes a 33 percent reduction in the original flange stress to 227 ksi, does not cause gaps on the inside of the joint, but almost doubles the gap on the outside of the joint from 8.3 mil to 15.7 mil (see Table VII). Slight increases are also noted in the gusset stress when the slots are cut in the flange and then the flange is split.

The results in Table IX also show that the magnitude of the stress concentration in the flange is directly related to the amount of material in the flange (most notably the flange thickness). The 170 and 180 stud designs with 3/4" thick flanges have maximum stress values which differ by only 1 percent. Increasing the flange thickness from 3/4" to 1" in the 170 stud design however, results in a 11.6 percent reduction in maximum flange stress.

The final item which will be discussed is the axial stress in the stud. In Table IX maximum axial stress in the stud at the symmetry plane Z = 0 is given for the preload condition as well as the full booster loading condition. For all cases shown, the axial stress in the stud is below the 195 ksi maximum defined previously. An unexpected phenomena however, is that under full loading, the maximum stud stress is less than or equal to the maximum stress due to just the preload alone. The full loading case causes opposing outside edges of the joint to peel away from each other which should try to stretch the stud and cause an increase in stress. At the same time however, the internal pressure is causing the flange to expand radially outward and lengthen. Since the flange is modeled with three dimensional solid elements, Poisson's ratio requires that the flange thickness decrease proportionally to the length increase. Any decrease in the flange thickness will relieve the stud prestress and this tends to negate or slightly overcome the increase in stud stress due to flange bending. As a result, stud stresses remain constant from the time the booster is assembled until firing is complete.

Mass and displaced volume - Although joint performance is of prime importance, joint mass also becomes a strong design driver because every pound of mass added to the SRM causes a reduction in shuttle payload capability to low Earth orbit. For the in-line bolted concept presented in this paper, key variables in minimizing the joint mass are using the smallest stud size possible, and minimizing the eccentricity required for acceptable joint

performance. Increasing the flange thickness beyond what is necessary to maintain acceptable stress levels will also drive the mass of this joint design rapidly upward.

In figure 23 the mass penalty is presented for in-line bolted joint concepts with various stud sizes. The mass penalties of the original tang-clevis which flew on mission 51-L (figure 1), and the proposed capture tang fix (figure 4) are calculated from dimensions given in reference 2 and are also shown. The mass penalty, which tells how much additional mass is required to cut a continuous cylindrical shell and then reassemble the pieces with a mechanical joint, is defined as the mass of the joint minus the mass of an equivalent length of straight booster shell. The proposed capture tang has a mass penalty of 932 lbm, which is 180 lbm greater than the penalty of the original joint. Figure 23 shows the advantage gained in using a larger number of smaller studs in the in-line bolted concept. The data points at 1" and 1 1/16" are calculated for the refined model presented in this report with design parameters; flange thickness = 3/4", bearing plate = 1/4", and eccentricity = -.5". The data point for a 1 1/4" stud diameter is for 144 studs and a flange thickness of 1" (with no bearing plate) as described in reference 3. The 180 - 1" stud design is 346 lbm heavier than the proposed capture tang fix and 526 lbm heavier than the original 51-L design. Further refinement and optimization can be used to remove additional mass from the in-line bolted joint design.

The three joint concepts; tang-clevis, capture tang, and in-line bolted, also displace volume on the inside of the booster, volume which could be used for propellant. The amount of volume displaced per joint is 2400 in^3 for the tang-clevis, 4000 in^3 for the capture tang, and 8100 in^3 for the in-line bolted design with 180 - 1" studs and eccentricity = -.5". Because of insulation on the inside of the case joint, each cubic inch of displaced volume does not necessarily displace a cubic inch of propellant. The actual propellant loss due to volume impingement would require a more refined analysis for each joint concept. Further refinements in the design which lead to reductions in both the alcove height and stud eccentricity will decrease the amount of propellant displaced by the in-line bolted concept.

CONCLUDING REMARKS

The structural design for an in-line bolted joint which can be used to connect Space Shuttle SRM case segments together is presented. The primary objective of the in-line bolted design is to keep the joint in the vicinity of the O-rings closed from the time the joint is assembled until SRM firing is complete. The in-line bolted design uses a static face seal between two precompressed flanges to eliminate the reliability issue associated with using gas pressure to seat the O-rings. Finally, the in-line bolted concept is much more amenable to analysis than current joint concepts because friction does not have to be modeled and all load paths are straightforward.

A large number of parametric analyses have been performed on detailed finite element models of the in-line bolted joint to characterize its structural behavior. Moving the stud centerline in towards the center of the booster (negative eccentricity) closes the inside of the joint where the

O-rings are located so that no gap exists during the entire duration of SRM firing. The number and size of studs used to connect the case segments also strongly influences joint performance with the gap on the inside of the joint decreasing as the size of the studs is decreased (and the corresponding number of studs is increased). Increasing the flange thickness does not reduce gaps on the inside of the joint where gap size is critical, but it does reduce gaps on the outside of the joint because of reduced flange bending.

Three regions in the joint have stresses which are higher than the calculated allowables. In two of the regions, material tailoring and model refinement will lead to stress levels which are acceptable. In the third region, the stress concentration occurs at the edge of the stud hole in the flange. This concentration is caused by inplane loading in the flange, which is due to the radial outward expansion of the SRM under the internal pressure loading. Several cycles of a plasticity analysis need to be run to assess the impact of this stress concentration on the in-line bolted design. If the stress concentration is found to be unacceptable, cutting slots in the flange is shown to be successful in reducing the magnitude of the stress concentration around the hole.

The mass of the in-line bolted joint concept, which is strongly influenced by design parameters, must be minimized if it is to be offered as an alternative to the current tang-clevis design. In general, minimum joint mass is achieved by using; 1) the smallest practical stud size, 2) the smallest offset between the stud centerline and shell wall centerline, and 3) the smallest values of flange and gussett thickness possible. Constraints on these parameters are dictated by the requirement to keep the inside of the joint (where the O-rings are located) closed, and to maintain acceptable stress levels throughout the joint. In the final design recommended here, the joint has 180-1" studs, an eccentricity of -.5", a flange thickness of 3/4", a bearing plate thickness of 1/4", and the stud is prestressed to 70 percent of its ultimate load. This joint has a mass penalty which is 526 lbm (per joint) over the 51-L design mass penalty and only 346 lbm (per joint) mass penalty over the proposed capture tang fix.

REFERENCES

1. Report of the Presidential Commission on the Space Shuttle Challenger Accident. Washington, D.C., June 6, 1986.

2. Greene, William H.; Knight, Norman F. Jr.; and Stockwell, Alan E.: Structural Behavior of the Space Shuttle SRM Tang-Clevis Joint. NASA TM-89018, September 1986.

3. Hedgepeth, Kenneth D.; et. al.: LaRC Conceptual Design of Solid Rocket Booster In-Line Bolted Joint. NASA TM-89046, December 1986.

4. Whetstone, W. D.: EISI-EAL Engineering Analysis Language Reference Manual - EISI-EAL System Level 312, Engineering Information Systems, Inc., August 1985.

5. SDRC I-DEAS GEOMOD - Solid Modeling and Design Reference Manual, Structural Dynamics Research Corporation, 1986.

6. SDRC I-DEAS SUPERTAB - Engineering Analysis Pre- and Post-Processing Reference Manual, Structural Dynamics Research Corporation, 1986.

TABLE I.- MATERIAL PROPERTIES.

	Nut and Bearing Plate	Stud	Shell Wall
Material	Inconel 718	MP 35N	D6AC
Tensile Ultimate Stress	265,000 psi	273,000 psi	195,000 psi
Tensile Yield Stress	215,000 psi	263,000 psi	180,000 psi
Young's Modulus	29.7×10^6 psi	35.9×10^6 psi	30.0×10^6 psi
Qualification	Orbiter	Orbiter	SRB

TABLE II.- STUD AND NUT PARAMETERS.

Stud Diameter	Nut Diameter	Stud Ultimate Strength	Nut Weight
1"	1.88"	182,700 lb	.330 lb
1 1/16"	1.99"	207,000 lb	.412 lb
1 1/8"	2.10"	234,200 lb	.493 lb
1 3/16"	2.22"	262,300 lb	.600 lb
1 1/4"	2.355"	292,000 lb	.713 lb

TABLE III.- GAP PERFORMANCE FOR FLANGES WITH AND WITHOUT A BEARING PLATE.

[170 - 1 1/16" studs, ϵ = -.5", Preload = 0.7 F_{ULT}]

Flange Characteristics	Gap, in				
	1070	1071	1080	1081	1085
Solid flange 1" thick	.0003	.0	.0003	.0001	.0046
3/4" thick flange with 1/4" bearing plate	.0	.0	.0	.0002	.0089
1" thick flange with 1/4" bearing plate	.0004	.0	.0004	.0002	.0040
1 1/4" thick flange with 1/4" bearing plate	.0004	.0	.0006	.0001	.0018

TABLE IV.- GAP PERFORMANCE VERSUS NUMBER OF STUDS.

[1" thick flange, ϵ = -.5", Preload = 0.7 F_{ULT}]

	Gaps, in			
	1070	1071	1080	1081
180 - 1" studs	.0001	.0	.0002	.0
170 - 1 1/16" studs	.0003	.0	.0003	.0001
166 - 1 1/16" studs	.0004	.0	.0004	.0002

TABLE V.- EFFECT OF FLANGE THICKNESS ON GAP PERFORMANCE.

[170 - 1 1/16" studs, ϵ = -.5", 1/4" bearing plate]

	Gaps, in							
	301	383	302	384	305	387	312	396
1" thick flange Flat side	.0	.0004	.0	.0003	.0	.0001	.0	.0044
3/4" thick flange O-ring side	.0001	.0002	.0	.0	.0	.0002	.0	.0092

TABLE VI.- GAP PERFORMANCE OF 170 AND 180 STUD DESIGNS.

[3/4" flange, 1/4" bearing plate, ϵ = -.5", O-ring side]

	Gaps, in							
	301	383	302	384	305	387	312	396
170 - 1 1/16"	.0001	.0002	.0	.0	.0	.0002	.0	.0092
180 - 1"	.0	.0	.0	.0	.0	.0002	.0	.0083

TABLE VII.- GAP PERFORMANCE FOR VARIOUS CASES OF A 180 - 1" STUD DESIGN.

[180 - 1" studs, 3/4" flange, 1/4" bearing plate]

Flange Characteristics	Gaps, in							
	301	383	302	384	305	387	312	396
O-ring side	.0	.0	.0	.0	.0	.0002	.0	.0083
Flat side	.0	.0	.0	.0	.0	.0002	.0	.0082
O-ring side with slots	.0	.0	.0	.0	.0	.0002	.0009	.0111
Flat side with slots	.0	.0	.0	.0	.0	.0004	.0008	.0110
O-ring side with slots with split flange	.0	.0	.0	.0	.0	.0	.0	.0157
Flat side with slots with split flange	.0	.0	.0	.0	.0	.0006	.0	.0154

TABLE VIII.- MAGNITUDE OF STRESSES ABOVE THE MAXIMUM ALLOWABLE.

[170 - 1 1/16" studs, ϵ = -.5", bearing plate = 1/4"]

	Stress, ksi			
Flange thickness, in	A (σ_Z)	B (σ_Y)	C1 (σ_Y)	C2 (σ_Y)
3/4	149.	185.	243.	278.
1	146.	—	228.	248.
1 1/4	143.	—	214.	227.

TABLE IX.- STRESSES IN THE REFINED MODEL.

Stud, flange specifications	σ_Z, ksi Stud		σ_Y, ksi Flange (location C)	σ_Z, ksi Gusset (location A)
	Preload	Full loading	Full loading	Full loading
170 - 1 1/16" studs 1" flange Flat side	172.	162.	298.	144.
170 - 1 1/16" studs 3/4" flange O-ring side	172.		337.	147.
180 - 1" studs 3/4" flange O-ring side	173.	167.	340.	155.
180 - 1" studs 3/4" flange Flat side			340.	155.
180 - 1" studs 3/4" flange O-ring side 2 slots cut	173.	173.	262.	157.
180 - 1" studs 3/4" flange O-ring side 2 slots cut Split flange		190.	227.	162.

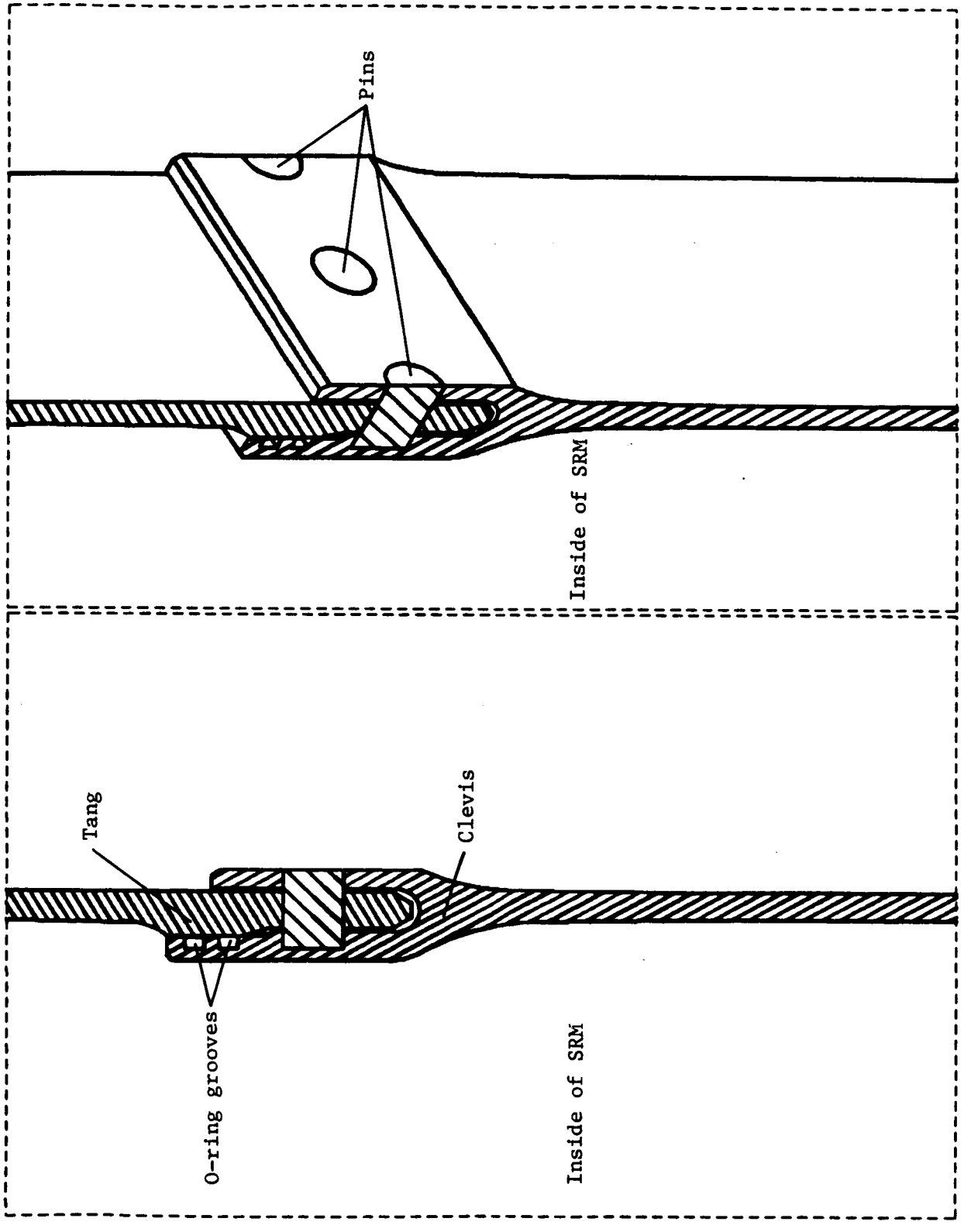

Figure 1.- Tang-clevis type field joint.

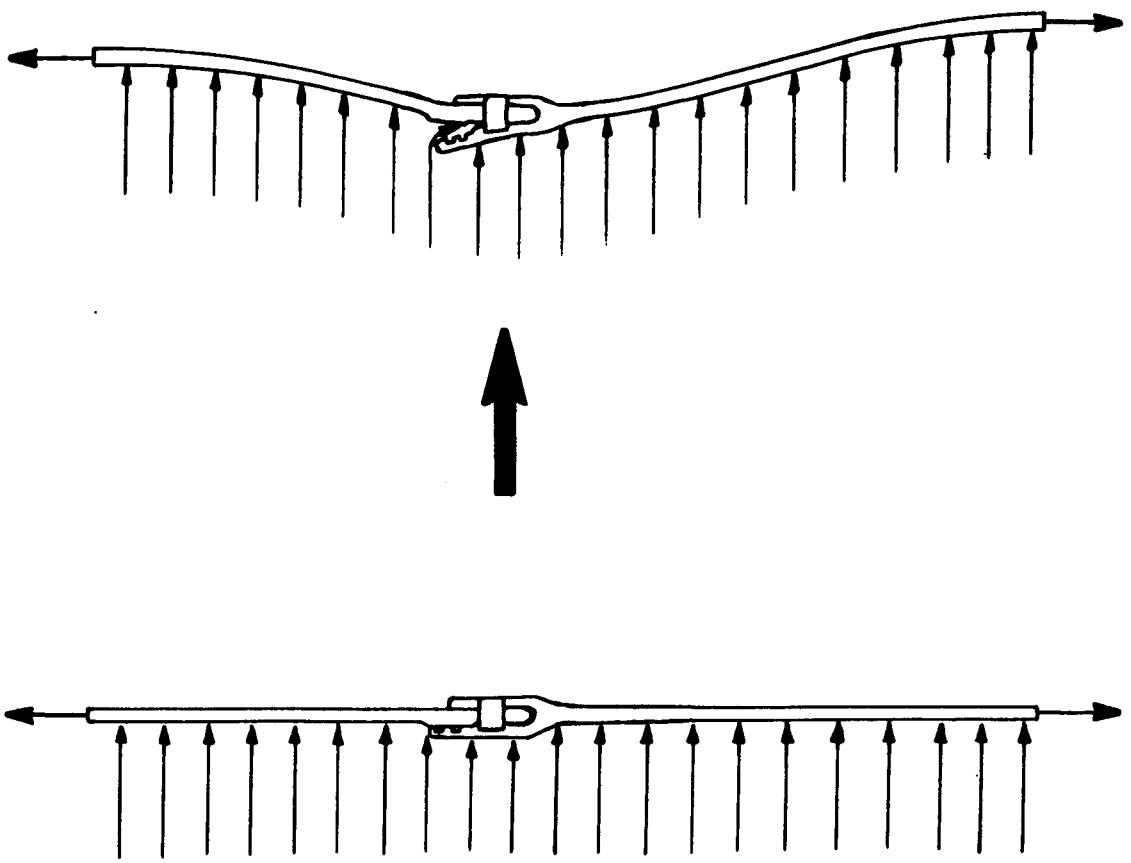

Figure 2.- Deflection shape of a tang-clevis joint due to internal pressure.

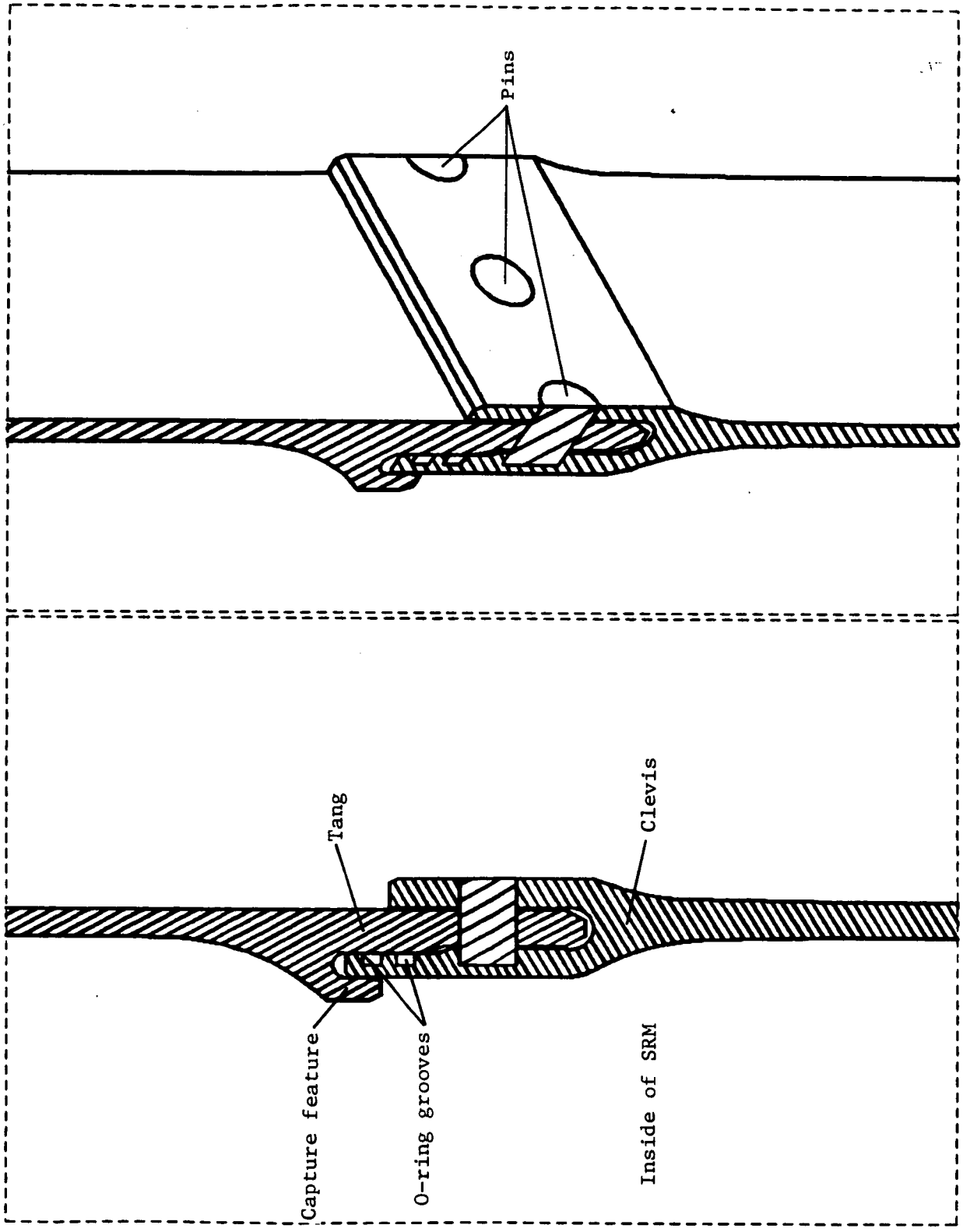

Figure 3.- Capture tang type field joint.

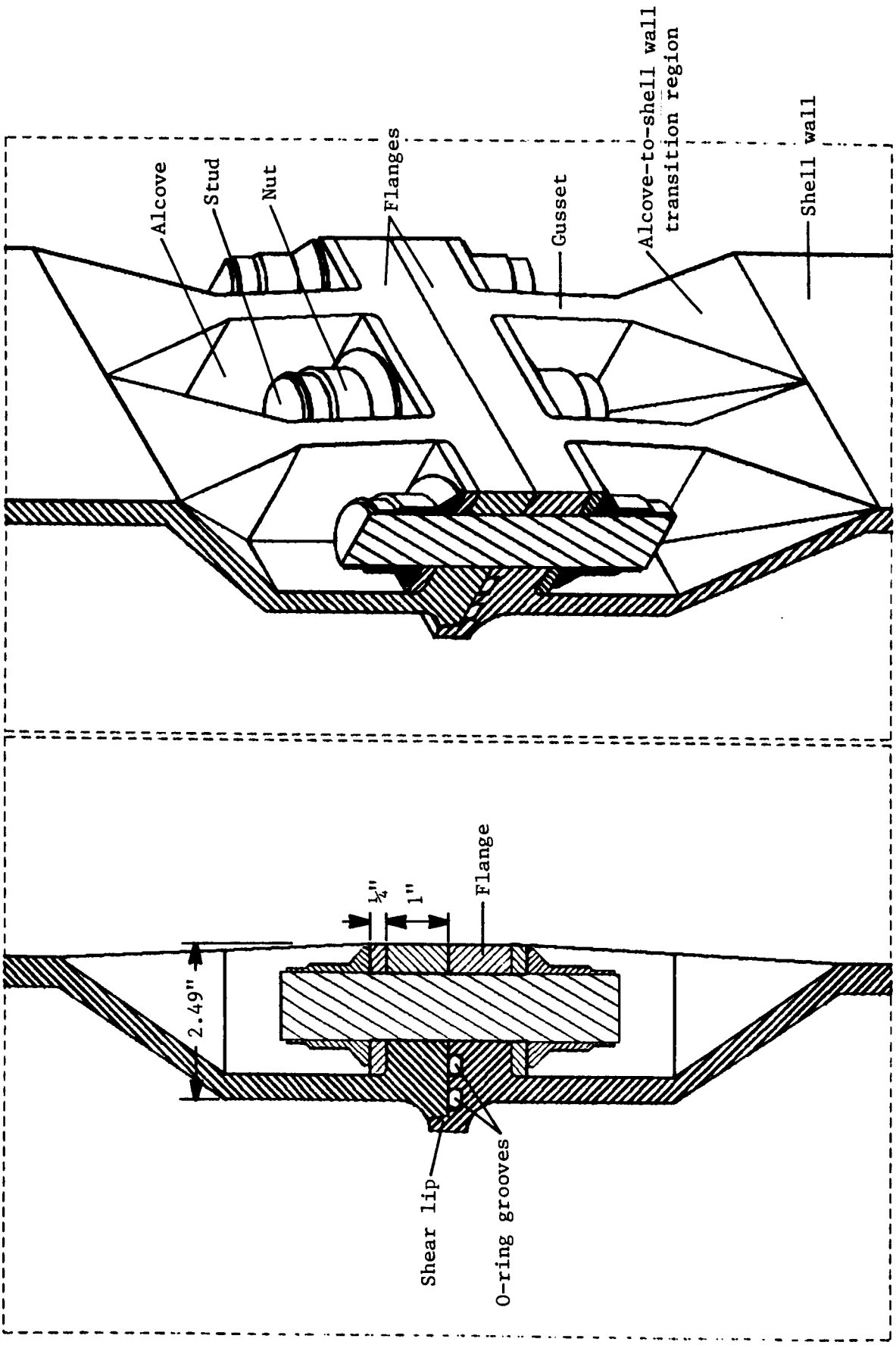

Figure 4.- In-line bolted joint concept.

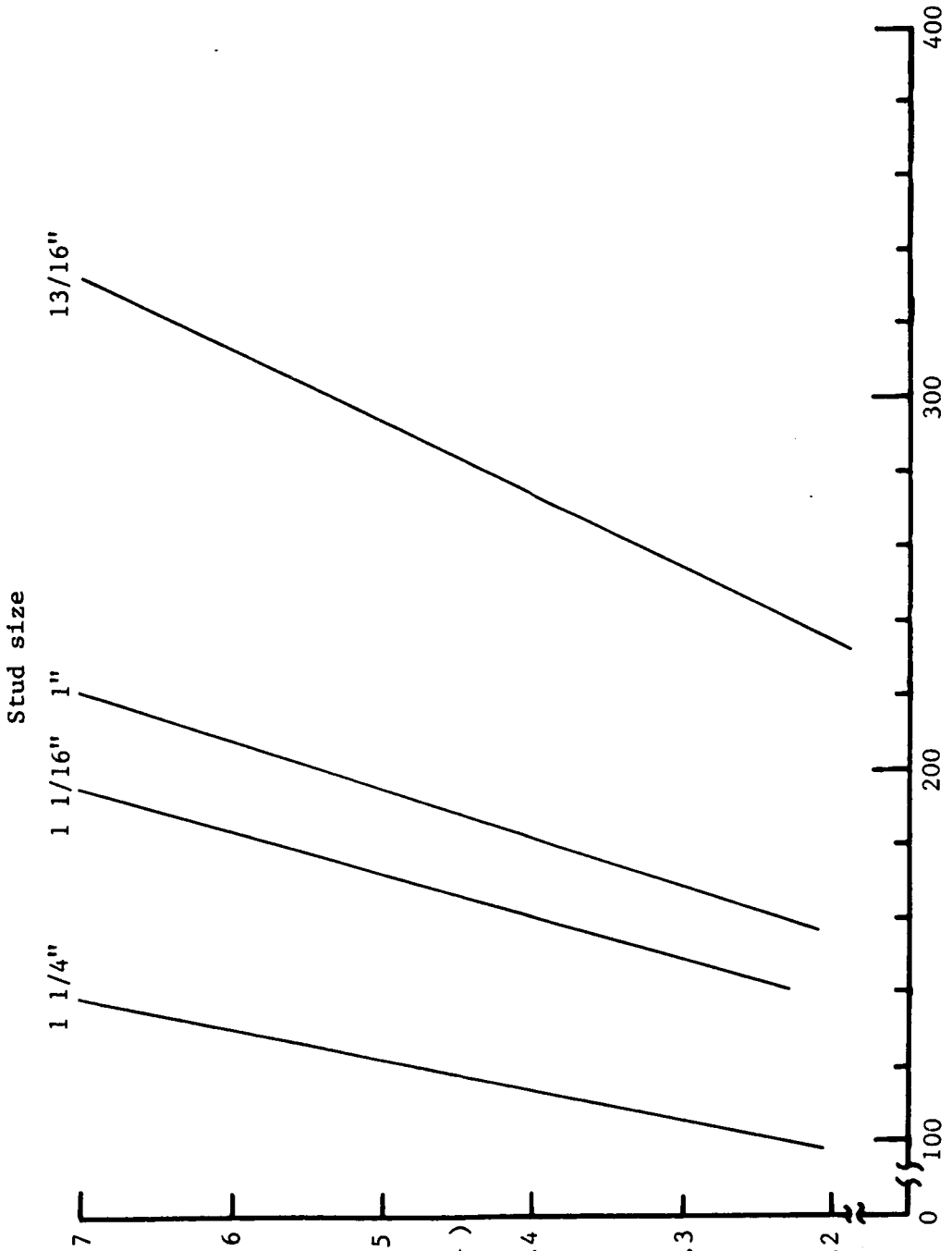

Figure 5.- Number of studs necessary to carry the axial load due to pressure.

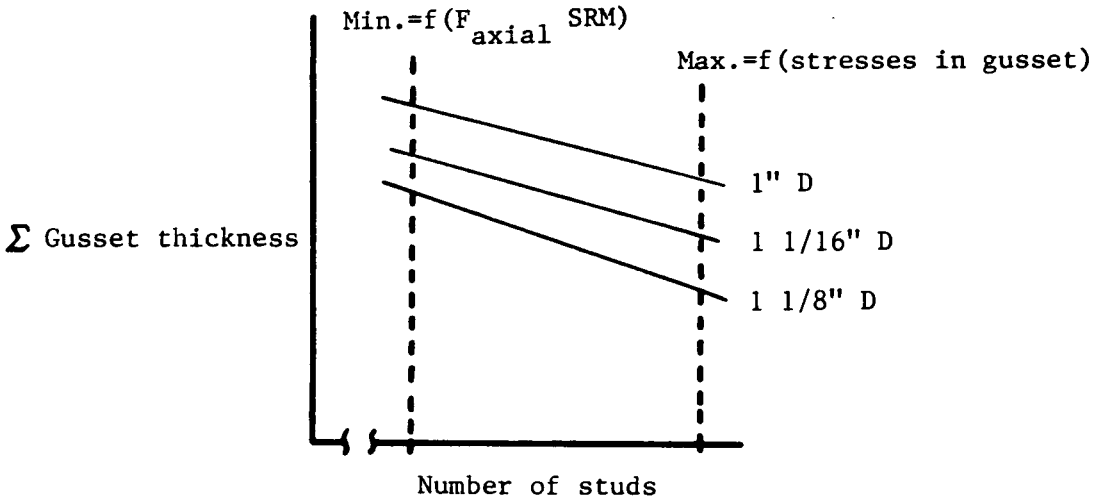

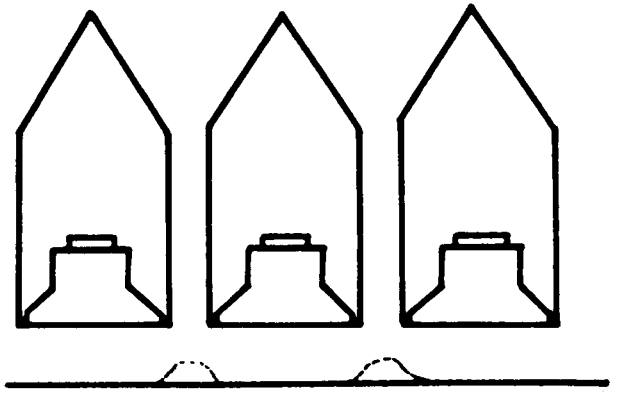

Scalloping between studs

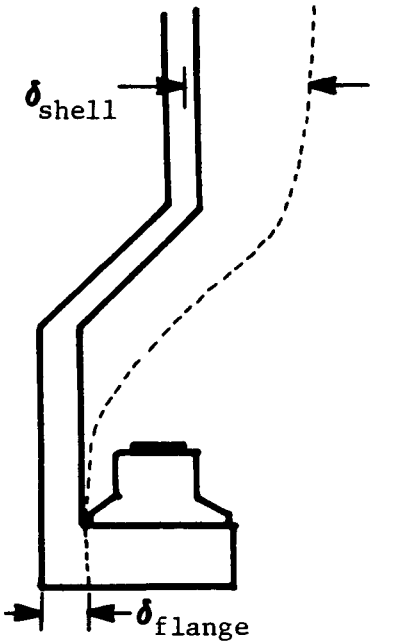

Hoop stiffness diferences

Figure 6.- Stud diameter and spacing affect joint performance.

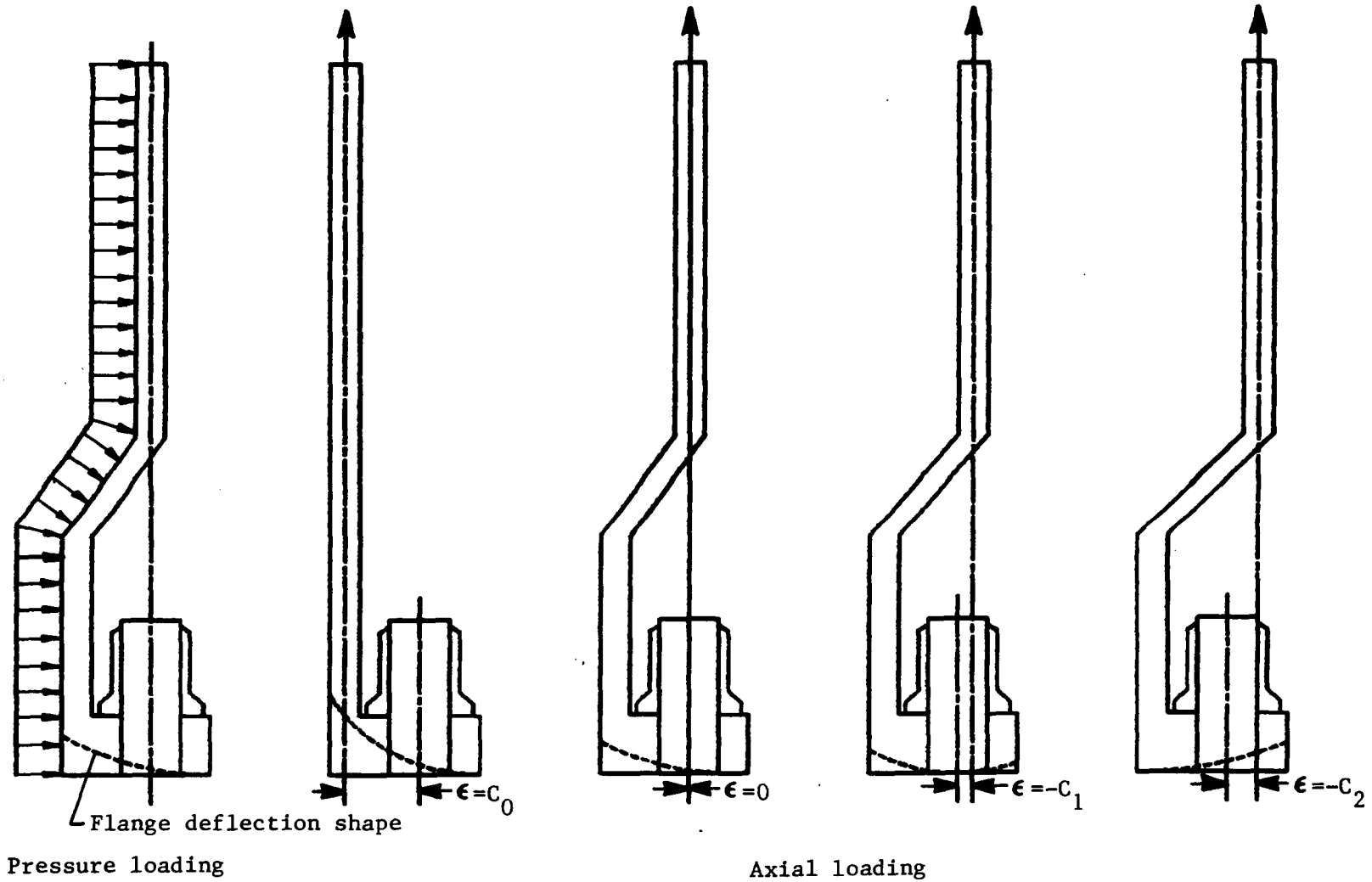

Figure 7.- Position of stud centerline (eccentricity) with respect to shell wall affects joint performance.

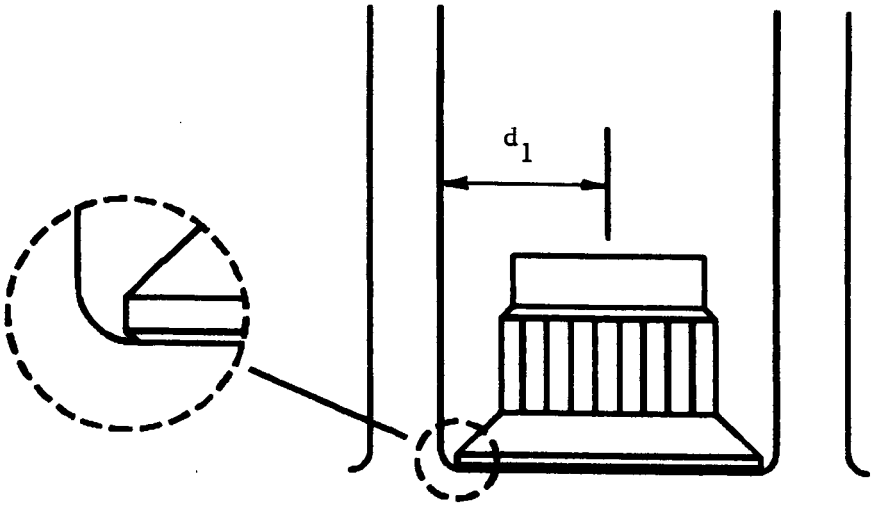

8a. No Bearing Plate

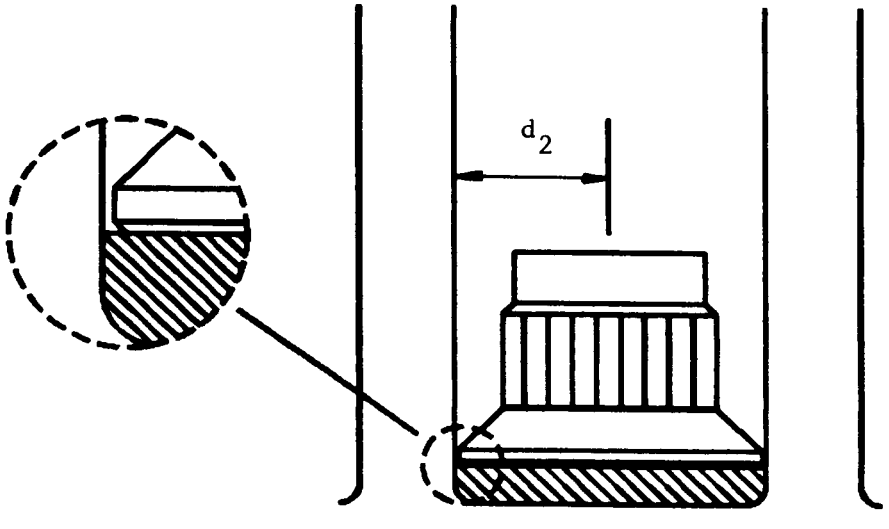

8b. Bearing Plate

Figure 8.- Effect of bearing plate on gusset thickness.

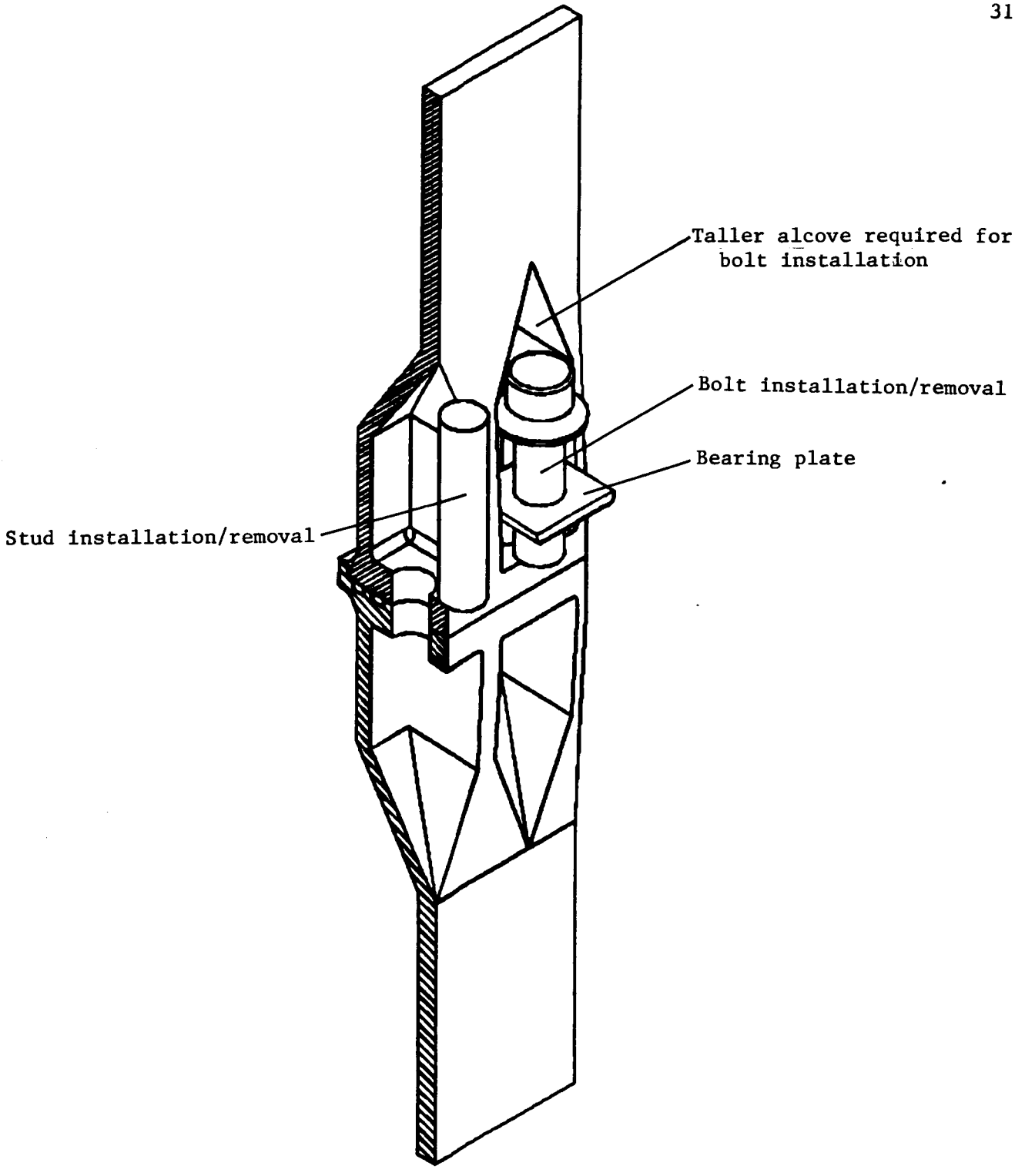

Figure 9.- Increase in alcove height required to install bolts instead of studs for in-line bolted joint concept.

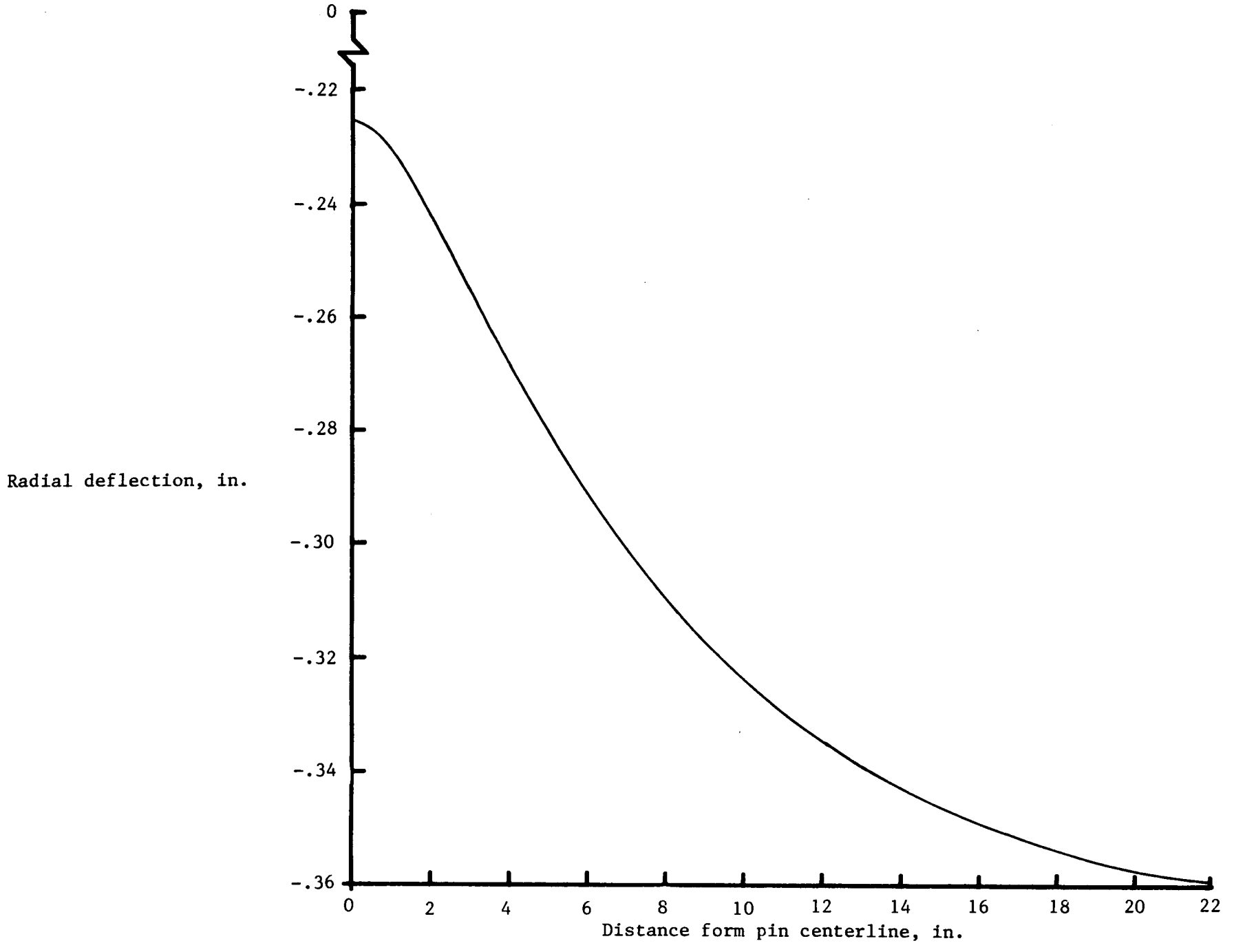

Figure 10.- Analysis of ring stiffened pressure vessel representing tang-clevis joint.

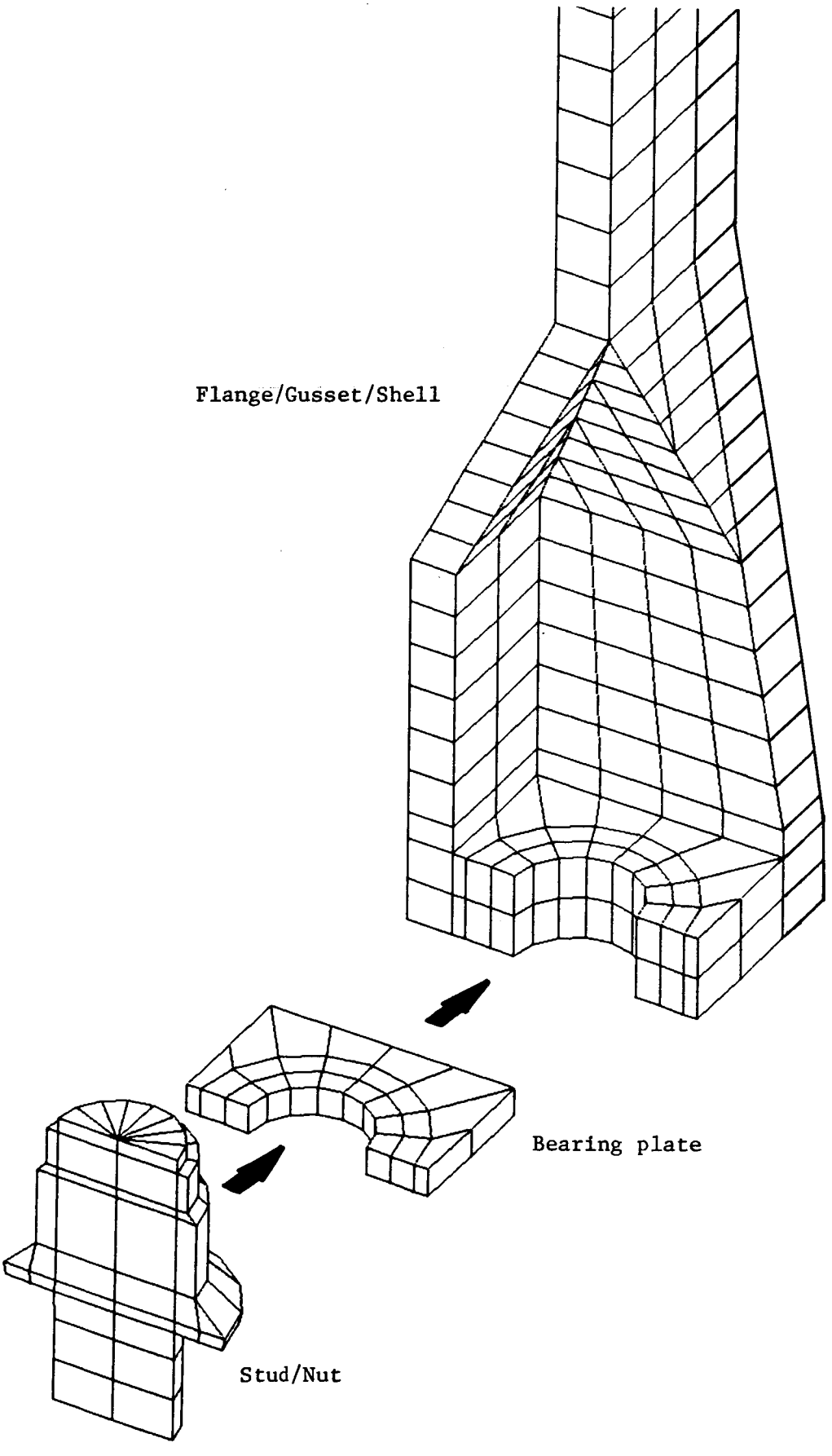

Figure 11.- Finite element subcomponent models.

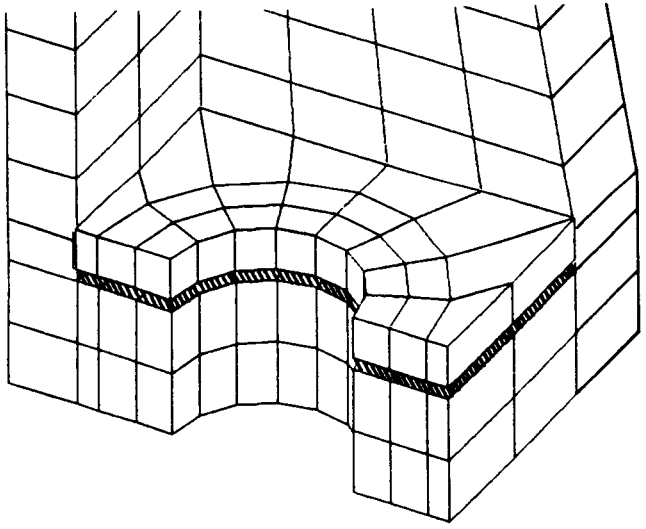

a. Bearing plate to flange assembly.

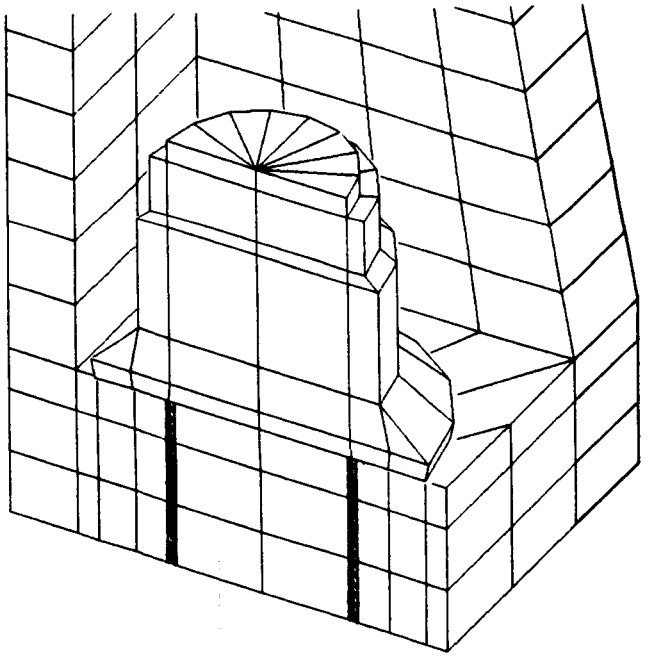

b. Stud/nut to flange/bearing plate assembly.

Gap element locations

Figure 12.- Finite element model assembly.

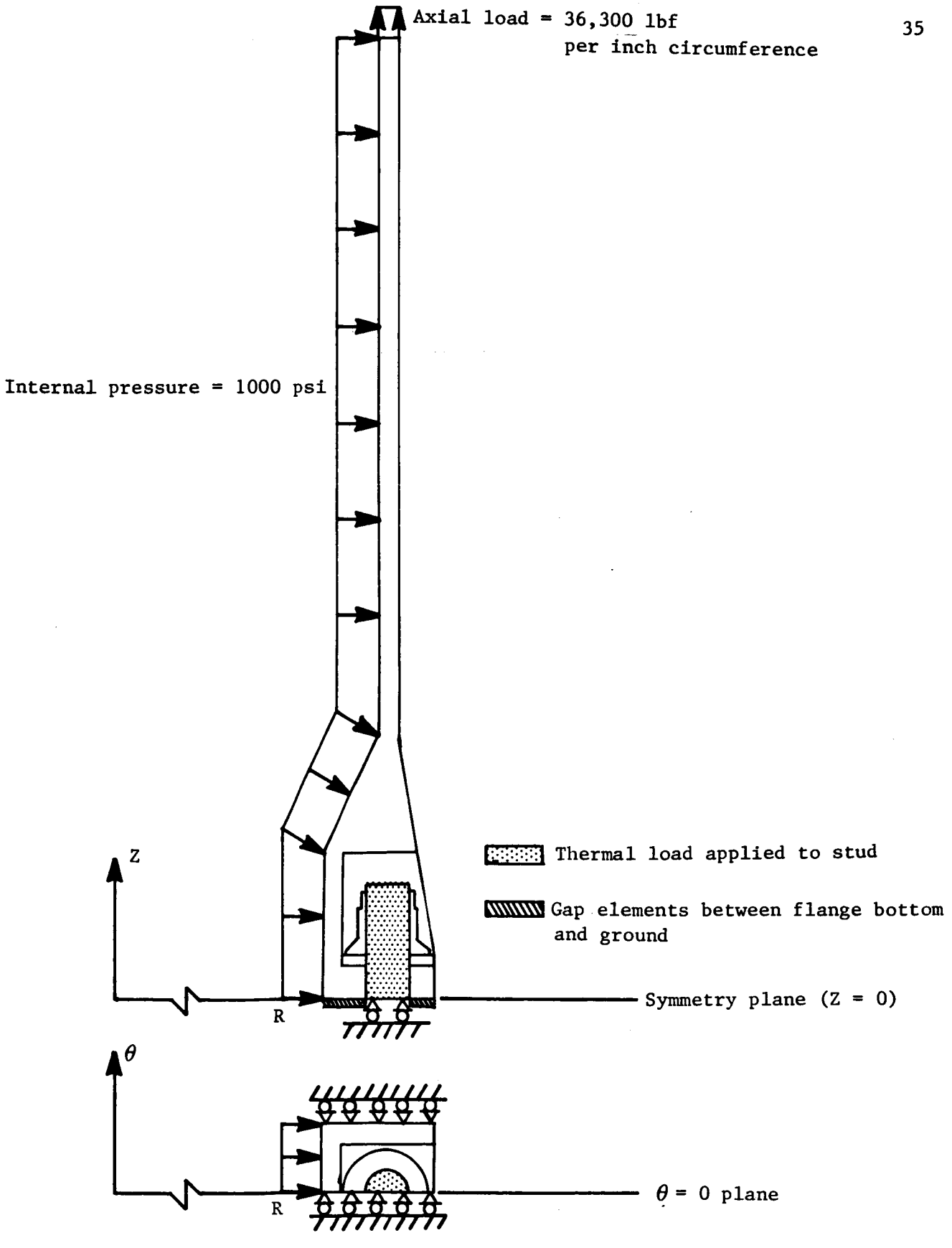

Figure 13.- Finite element model boundary conditions and applied loadings.

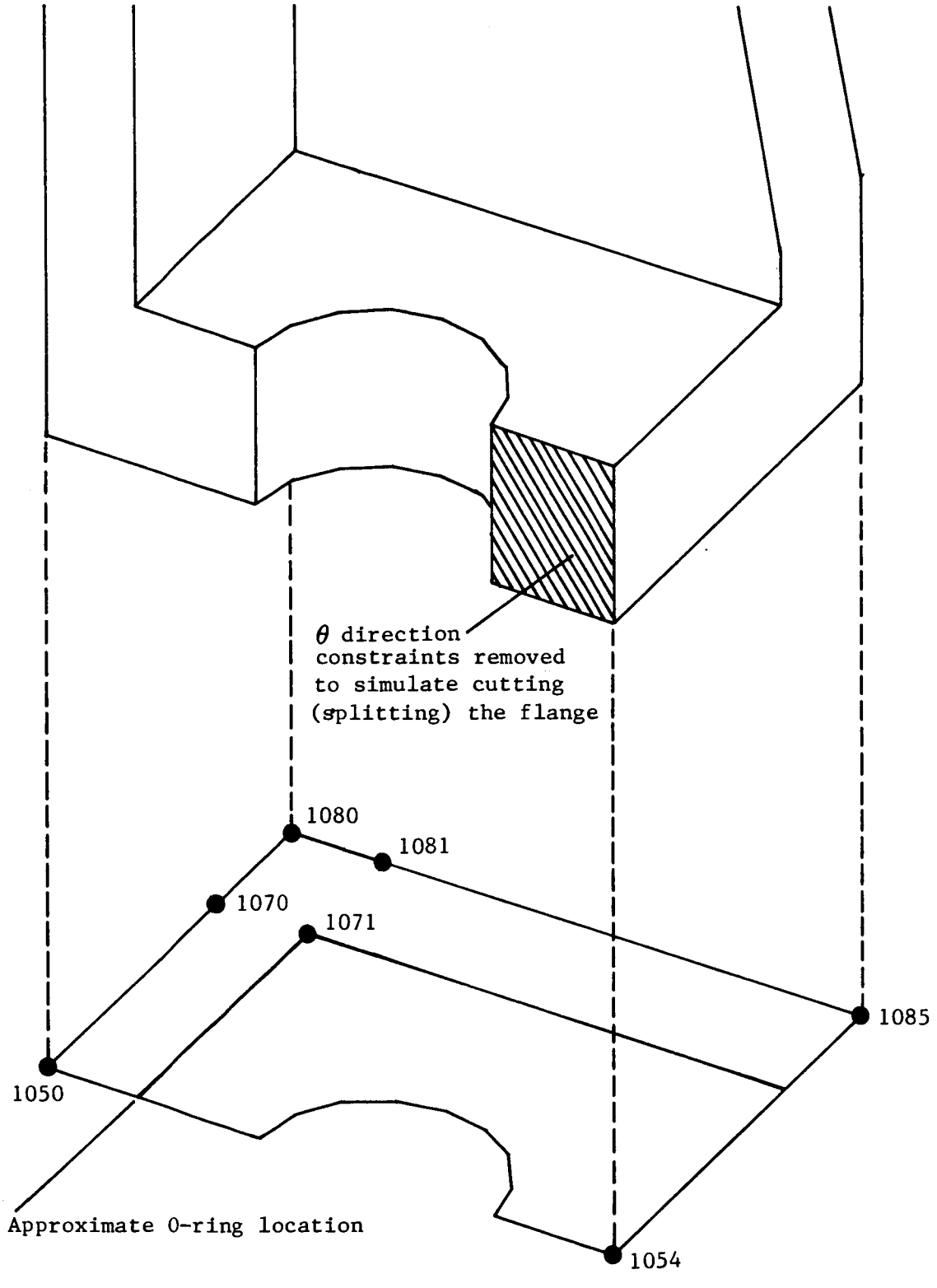

Figure 14.- Gap locations monitored on flange bottom.

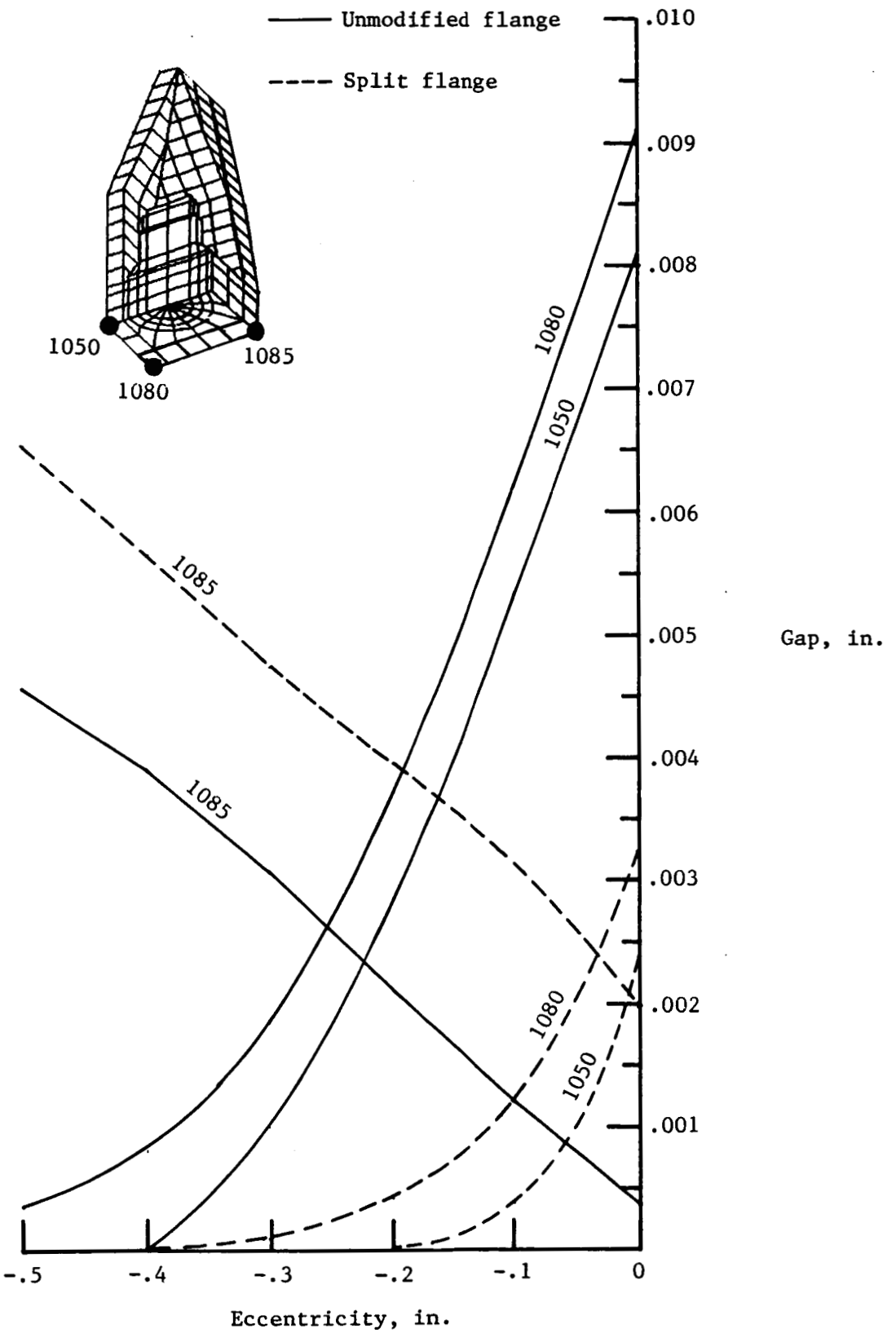

Figure 15.- Gap magnitudes on flange bottom versus stud eccentricity.

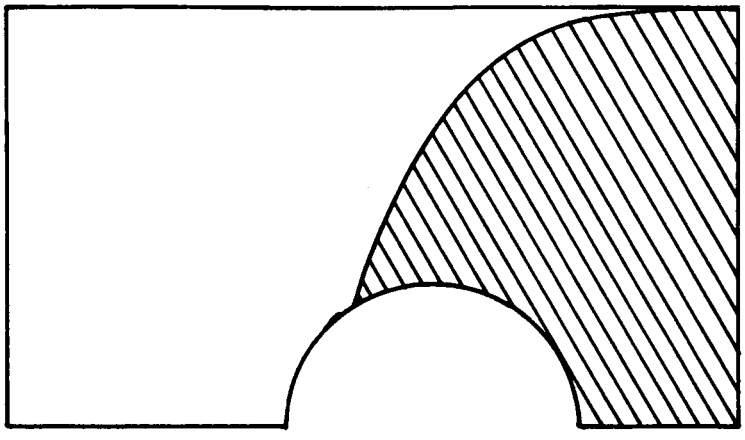

a. Eccentricity = 0 in.

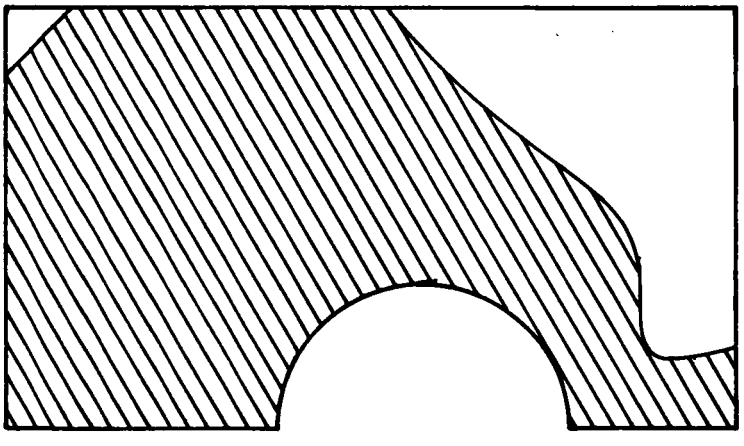

b. Eccentricity = -.5 in.

Figure 16.- Contact region on flange bottom for two values of stud eccentricity.

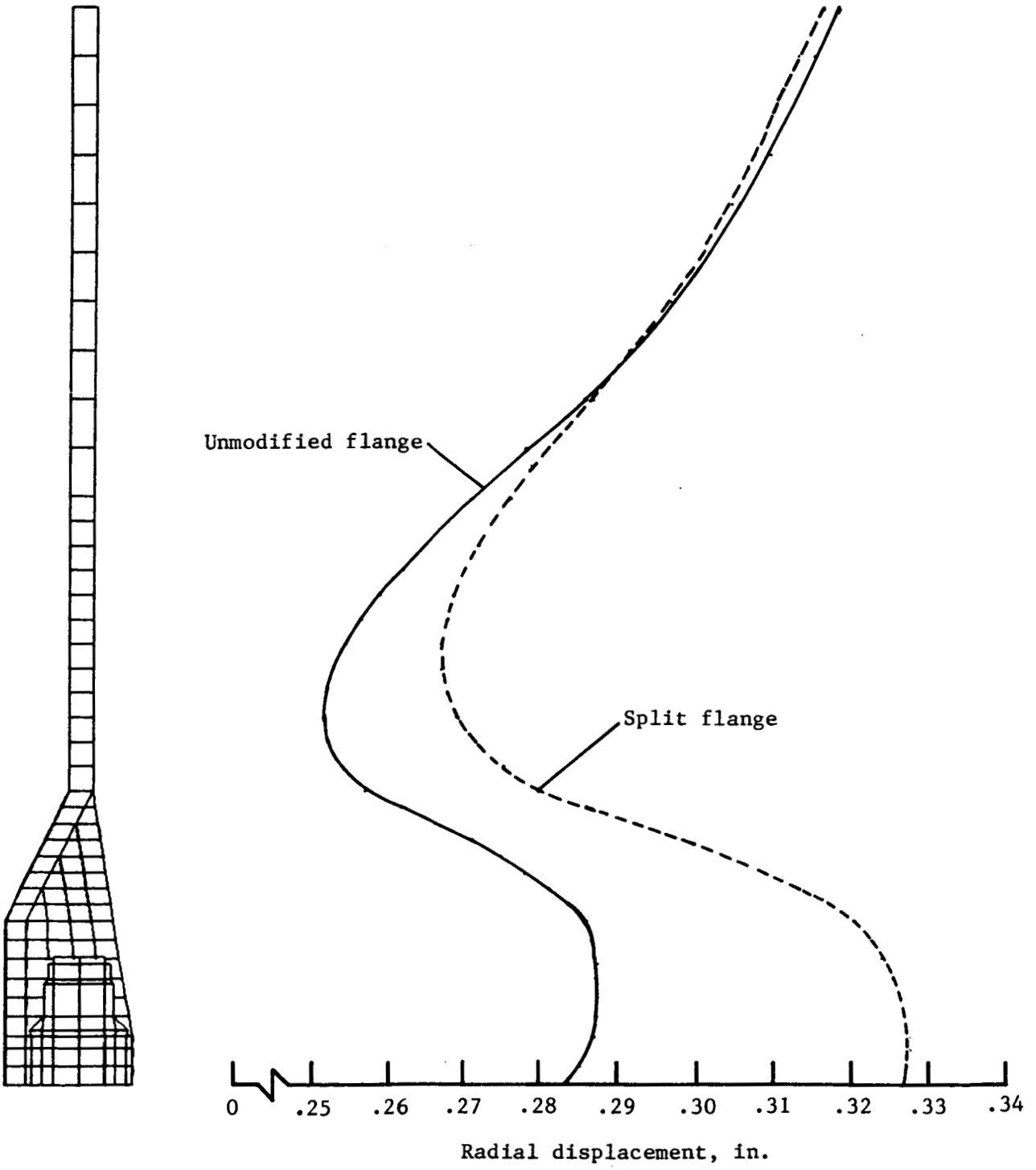

Figure 17.- Reduction in flange hoop stiffness achieved by splitting flange.

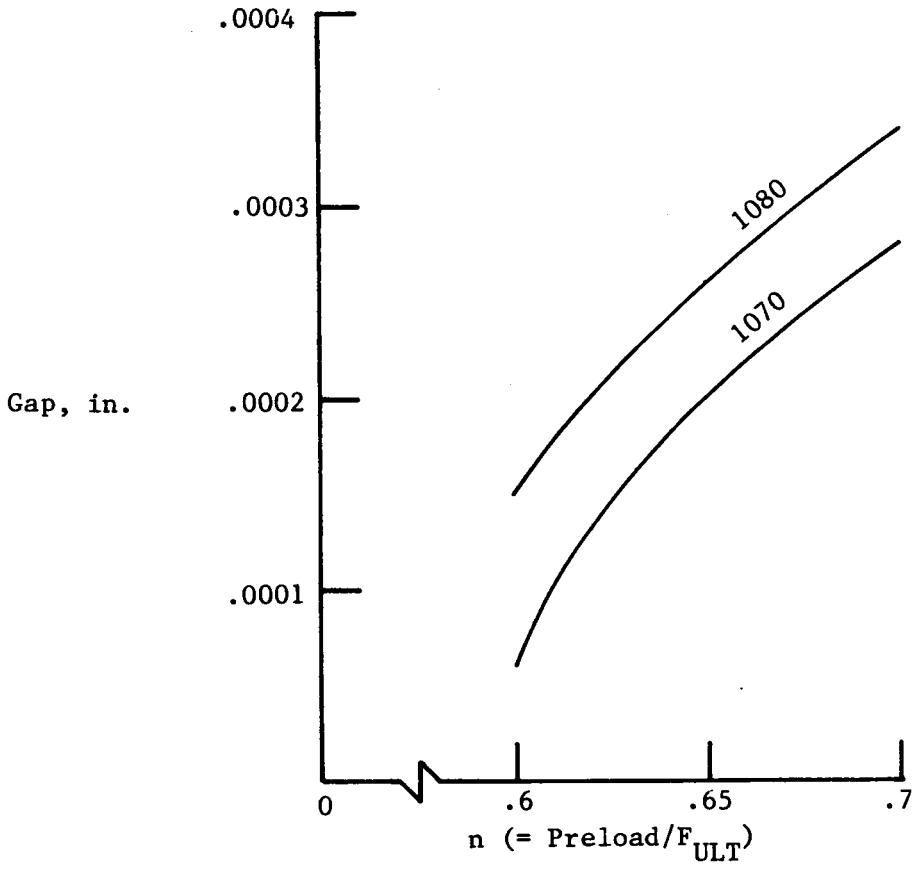

a. Locations on inside of joint.

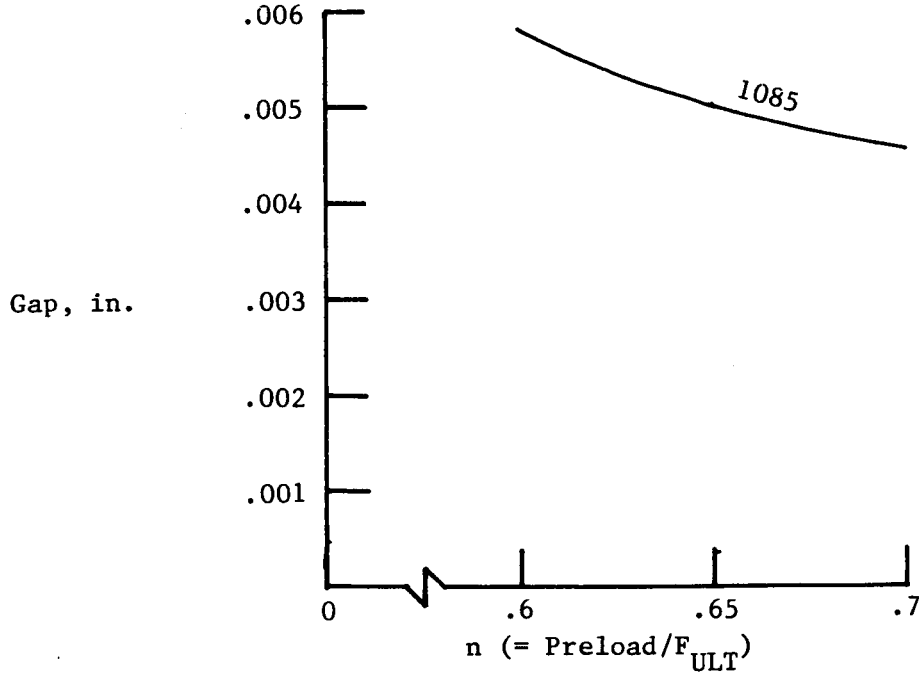

b. Location on outside of joint.

Figure 18.- Gap magnitude on flange bottom versus initial stud preload.

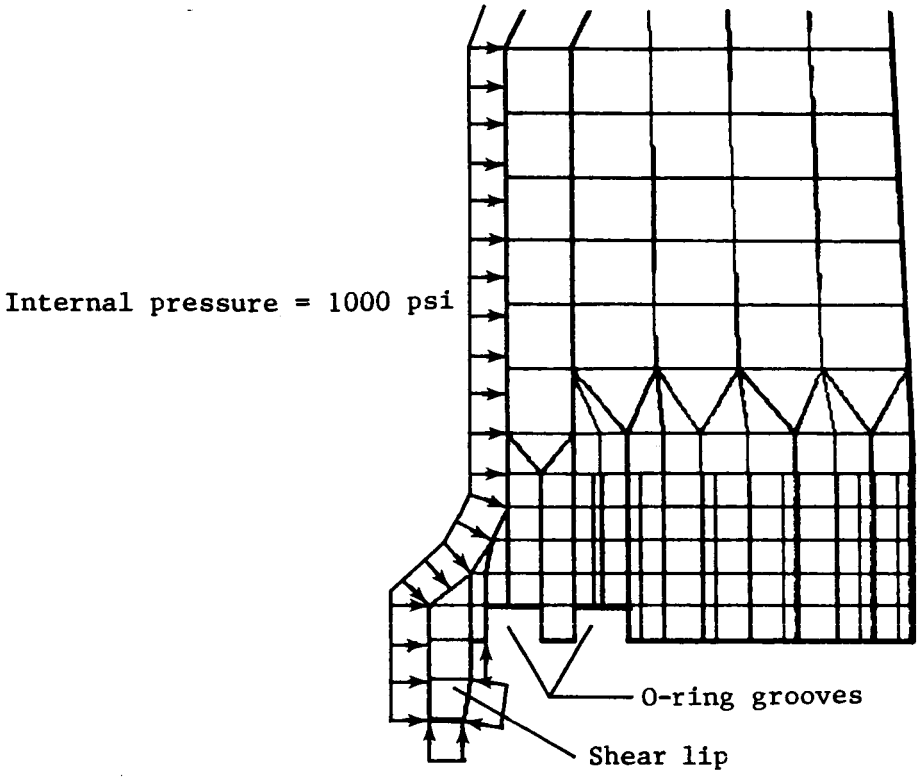

19a. O-ring side.

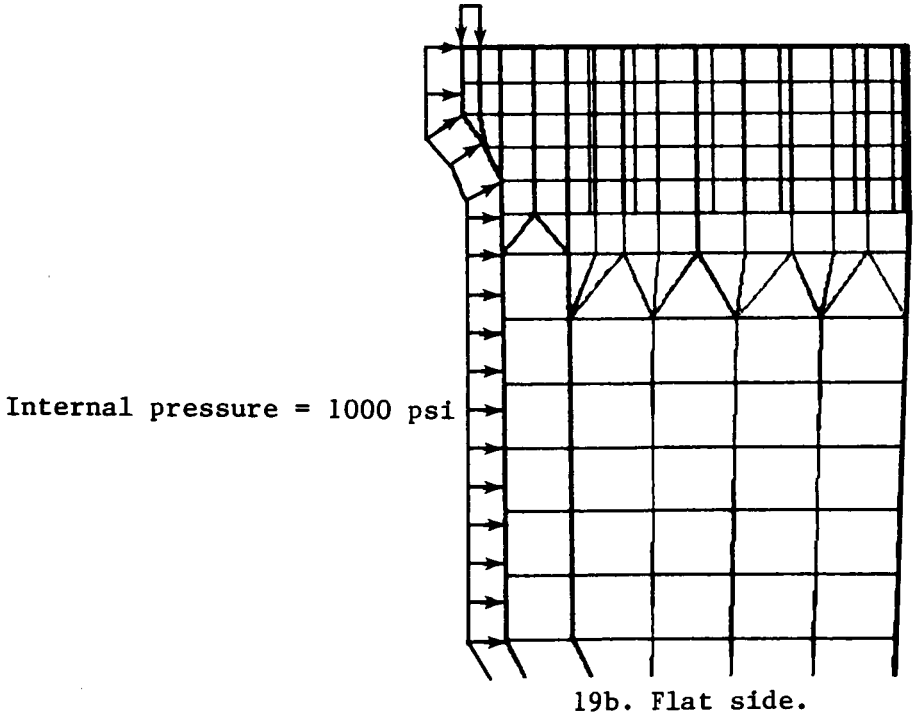

19b. Flat side.

Figure 19.- Refined finite element model.

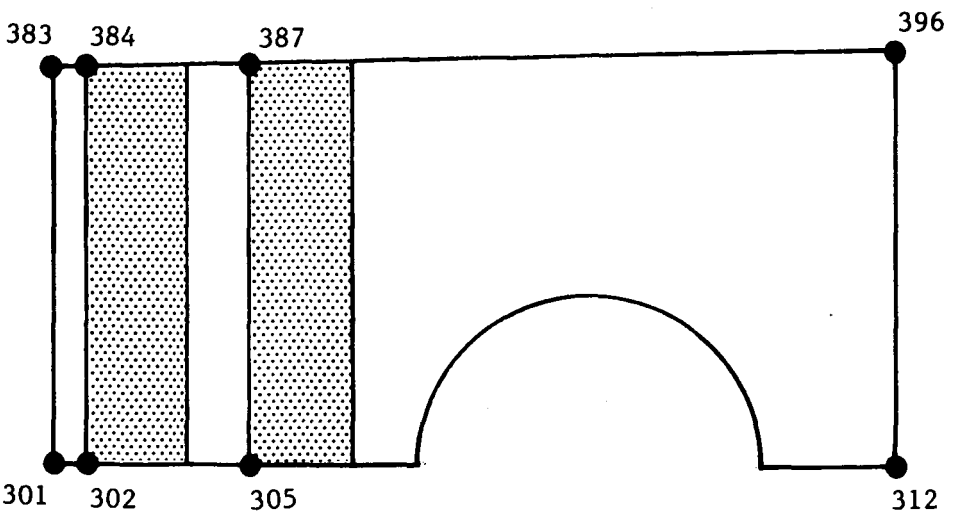

Figure 20.- Gap locations monitored on flange bottom of refined model.

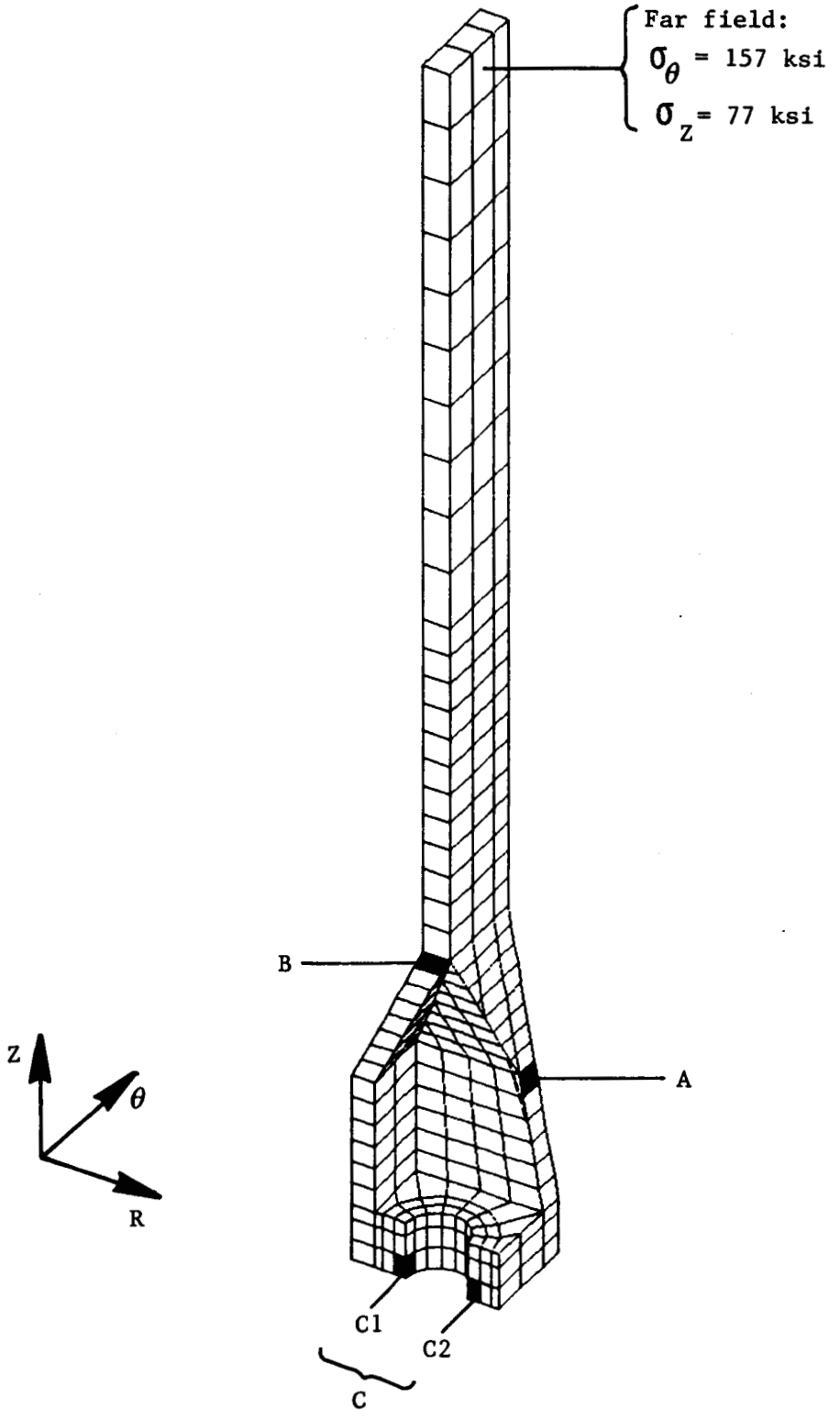

Figure 21.- Locations where stresses are above the maximum allowable.

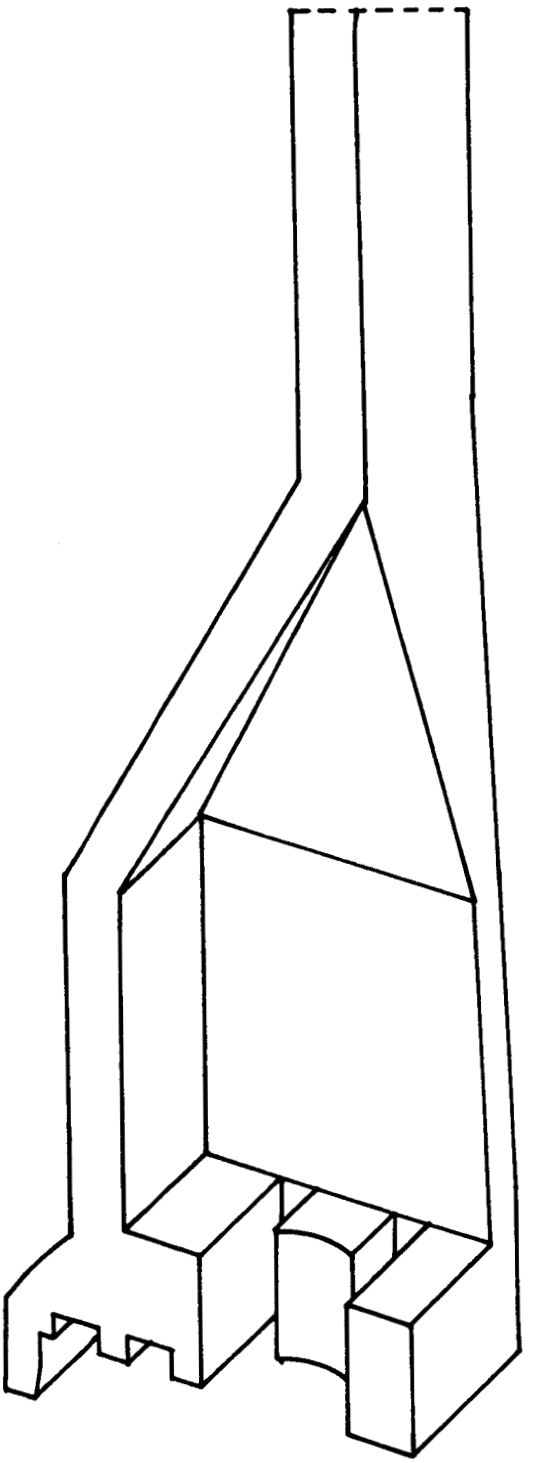

Figure 22.- Slots cut in flange to reduce stress concentration around the stud hole.

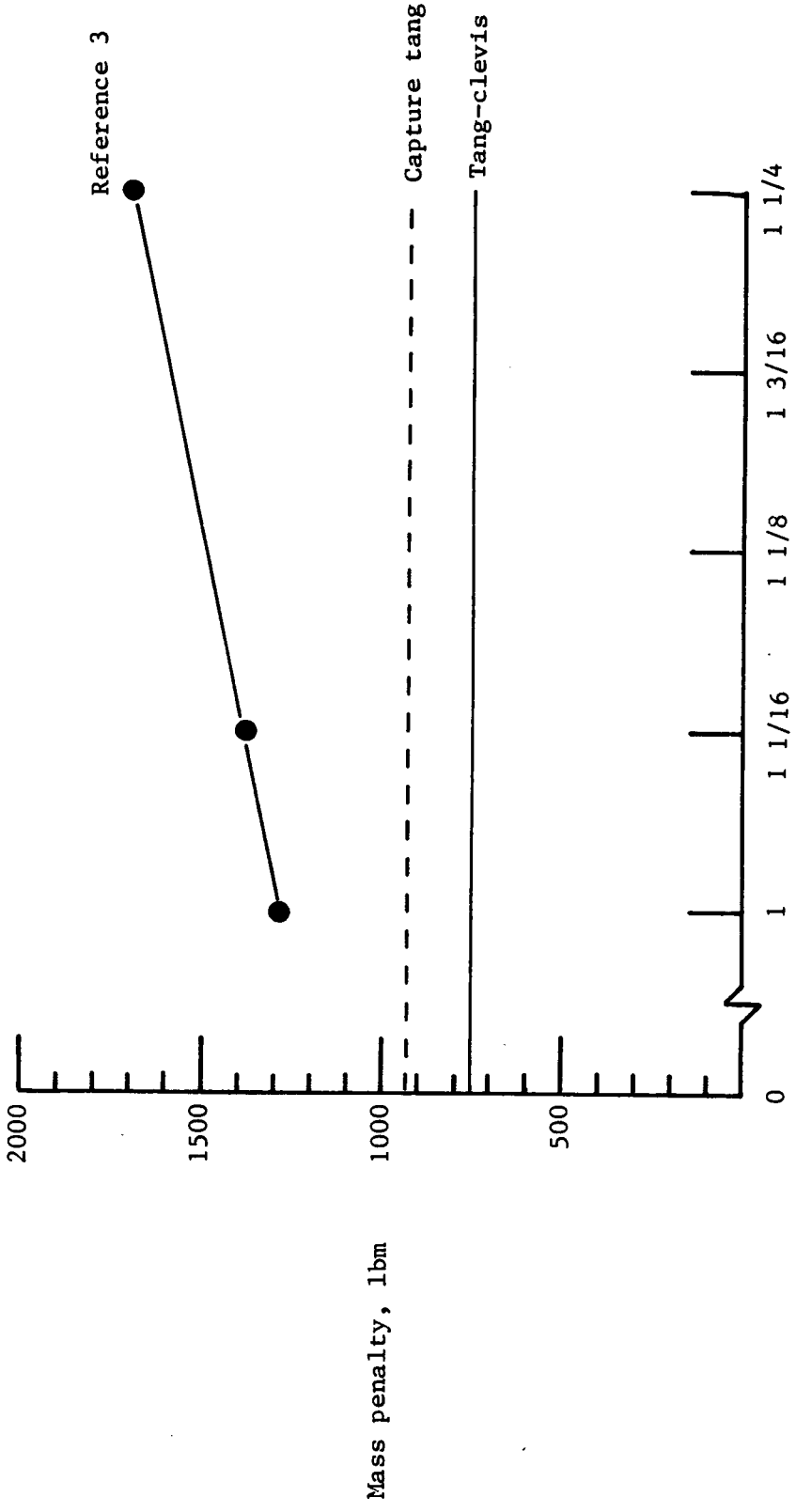

Figure 23.- Mass penalty per joint for various case segment joint designs.

1. Report No.	2. Government Accession No.	3. Recipient's Catalog No.
NASA TM-89027		

4. Title and Subtitle	5. Report Date
Structural Design of an In-line Bolted Joint for the Space Shuttle Solid Rocket Motor Case Segments	March 1987
	6. Performing Organization Code: 506-43-41-02

7. Author(s)	8. Performing Organization Report No.
John T. Dorsey, Peter A. Stein, and Harold G. Bush	
	10. Work Unit No.

9. Performing Organization Name and Address	11. Contract or Grant No.
NASA Langley Research Center Hampton, VA 23665-5225	
	13. Type of Report and Period Covered: Technical Memorandum

12. Sponsoring Agency Name and Address	14. Sponsoring Agency Code
National Aeronautics and Space Administration Washington, DC 20546	

15. Supplementary Notes

16. Abstract

This paper presents results of a structural design study of an in-line bolted joint concept which can be used to assemble Space Shuttle Solid Rocket Motor (SRM) case segments. Numerous parametric studies are performed to characterize the in-line bolted joint behavior as major design variables are altered, with the primary objective always being to keep the inside of the joint (where the O-rings are located) closed during the SRM firing. The resulting design has 180-1 inch studs, an eccentricity of -0.5 inch, a flange thickness of 3/4 inch, a bearing plate thickness of 1/4 inch, and the studs are subjected to a preload which is 70 percent of ultimate. The mass penalty per case segment joint for the in-line design is 346 lbm more than the weight penalty for the proposed capture tang fix.

17. Key Words (Suggested by Author(s))	18. Distribution Statement
Space Shuttle Solid Rocket Motor (SRM) In-line Bolted Joint SRM Case Segment Field Joint	Unclassified - Unlimited Subject Category 18

19. Security Classif. (of this report)	20. Security Classif. (of this page)	21. No. of Pages	22. Price
Unclassified	Unclassified	46	A03

For sale by the National Technical Information Service, Springfield, Virginia 22161